1995-12

Modeling and experimental testing for future development of Night Vision Electro-Optic (NVEO) FLIR92 Model

Koc, Cem.

Monterey, California. Naval Postgraduate School

http://hdl.handle.net/10945/7464

NAVAL POSTGRADUATE SCHOOL
Monterey, California

THESIS

MODELING AND EXPERIMENTAL TESTING FOR FUTURE DEVELOPMENT OF NIGHT VISION ELECTRO-OPTIC (NVEO) FLIR92 MODEL

by

Cem Koc

December, 1995

Thesis Advisor: Ron J. Pieper
Co-Advisor : Alfred W. Cooper

Approved for public release; distribution is unlimited.

REPORT DOCUMENTATION PAGE			Form Approved OMB No. 0704-0188
Public reporting burden for this collection of information is estimated to average 1 hour per response, including the time for reviewing instruction, searching existing data sources, gathering and maintaining the data needed, and completing and reviewing the collection of information. Send comments regarding this burden estimate or any other aspect of this collection of information, including suggestions for reducing this burden, to Washington Headquarters Services, Directorate for Information Operations and Reports, 1215 Jefferson Davis Highway, Suite 1204, Arlington, VA 22202-4302, and to the Office of Management and Budget, Paperwork Reduction Project (0704-0188) Washington DC 20503.			
1. AGENCY USE ONLY *(Leave blank)*	2. REPORT DATE December 1995	3. REPORT TYPE AND DATES COVERED Master's Thesis	
4. TITLE AND SUBTITLE MODELING AND EXPERIMENTAL TESTING FOR FUTURE DEVELOPMENT OF NIGHT VISION ELECTRO-OPTIC (NVEO) FLIR92 MODEL			5. FUNDING NUMBERS
6. AUTHOR(S) Koc, Cem			
7. PERFORMING ORGANIZATION NAME(S) AND ADDRESS(ES) Naval Postgraduate School Monterey CA 93943-5000			8. PERFORMING ORGANIZATION REPORT NUMBER
9. SPONSORING/MONITORING AGENCY NAME(S) AND ADDRESS(ES)			10. SPONSORING/MONITORING AGENCY REPORT NUMBER
11. SUPPLEMENTARY NOTES The views expressed in this thesis are those of the author and do not reflect the official policy or position of the Department of Defense or the U.S. Government.			
12a. DISTRIBUTION/AVAILABILITY STATEMENT Approved for public release; distribution is unlimited.			12b. DISTRIBUTION CODE

13. ABSTRACT *(maximum 200 words)*

Recent advances in thermal imaging technology have resulted in the fielding of two- dimensional array detector based imaging systems. These designs have been labeled second-generation, and are rapidly replacing first generation systems having linear detector arrays with a parallel scan type architecture. It has been postulated that first generation prediction models are not applicable to second generation systems. In particular, the minimum resolvable temperature difference (MRTD)modeling needs refinement in the areas of sampling, quantization noise, and array non-uniformities in order for it to be applied to second generation systems. The present industry standard for MRTD is the Night Vision FLIR92 Model. Results from the FLIR92 Model and the two well known first generation models will be presented and compared with experimental measurements made on two thermal imaging systems available at the Naval Postgraduate School.

14. SUBJECT TERMS Thermal Imaging Systems, FLIR Performance, Minimum Resolvable Temperature Difference (MRTD)			15. NUMBER OF PAGES 130
			16. PRICE CODE
17. SECURITY CLASSIFICATION OF REPORT Unclassified	18. SECURITY CLASSIFICATION OF THIS PAGE Unclassified	19. SECURITY CLASSIFICATION OF ABSTRACT Unclassified	20. LIMITATION OF ABSTRACT UL

NSN 7540-01-280-5500

Standard Form 298 (Rev. 2-89)
Prescribed by ANSI Std. 239-18 298-102

Approved for public release; distribution is unlimited.

MODELING AND EXPERIMENTAL TESTING FOR FUTURE DEVELOPMENT OF NIGHT VISION ELECTRO-OPTIC (NVEO) FLIR92 MODEL

Cem Koc
Lieutenant Junior Grade, Turkish Navy
B.S.E.E., Turkish Naval Academy, 1989

Submitted in partial fulfillment
of the requirements for the degree of

MASTER OF SCIENCE IN SYSTEMS ENGINEERING
(ELECTRONIC WARFARE)
from the

NAVAL POSTGRADUATE SCHOOL
December 1995

Author: [redacted]
Cem Koc

Approved by: [redacted]
Ron J. Pieper, Thesis Advisor

[redacted]
Alfred W. Cooper, Co-Advisor

[redacted]
Frederic H. Levien, Chairman,
Electronic Warfare Academic Group

ABSTRACT

Recent advances in thermal imaging technology have resulted in the fielding of two-dimensional array detector based imaging systems. These designs have been labeled second-generation, and are rapidly replacing first generation systems having linear detector arrays with a parallel scan type architecture. It has been postulated that first generation prediction models are not applicable to second generation systems. In particular, the minimum resolvable temperature difference (MRTD) modeling needs refinement in the areas of sampling, quantization noise, and array non-uniformities in order for it to be applied to second generation systems. The present industry standard for MRTD is the Night Vision FLIR92 Model. Results from the FLIR92 Model and the two well known first generation models will be presented and compared with experimental measurements made on two thermal imaging systems available at the Naval Postgraduate School.

TABLE OF CONTENTS

I. INTRODUCTION....................1
A. REVIEW OF LITERATURE....................1
B. OVERVIEW OF THE THESIS....................4
C. FUNDAMENTALS OF THERMAL IMAGING SYSTEMS....................5
D. BASIC PARAMETERS OF THERMAL IMAGING SYSTEMS....................6
E. JOHNSON CRITERION....................13
F. MOTIVATION FOR THIS WORK....................14

II. FIRST GENERATION THERMAL IMAGING SYSTEMS....................15
A. SAMPLE SYSTEM....................15
B. THE EYE-BRAIN MODELS....................15
C. NETD....................16
D. MRTD....................17

III. U.S. ARMY NVSED FLIR92 TIS PERFORMANCE MODEL....................25
A. MTFs....................25
B. NOISE....................27
C. MRTD AND MDTD....................35

IV. ALIASING....................41
A. MODEL....................41
B. ANALYSIS AND SIMULATION OF THE ALIASING....................46
C. REDUCING THE ALIASING EFFECT....................56

V. LABORATORY MEASUREMENTS....................59
A. LABORATORY SETUP....................59
B. PROCEDURE....................62
C. EXPERIMENTAL MRTD MEASUREMENTS....................62

D. OBJECTIVE MEASUREMENTS....65

VI. COMPARISON OF FLIR92 MRTD TO MEASURED MRTD AND CONCLUSION....69
A. COMPARISON OF FLIR92 MRTD TO MEASURED MRTD....69
B. LIMITATIONS OF THE FLIR92 AND CONCLUSION....73

APPENDIX A -THERMAL IMAGING SYSTEM PARAMETERS....75

APPENDIX B - FLIR92 MTF EQUATIONS AND D OPERATOR....79

APPENDIX C - LABORATORY MEASUREMENTS....85

APPENDIX D - FLIR92 SHORT-LISTING OUTPUTS....93

LIST OF REFERENCES....109

INITIAL DISTRIBUTION LIST....113

TABLE OF SYMBOLS

ε	: Charge transfer efficiency
Δf_n	: Noise equivalent electrical bandwidth (Hz)
Δf_p	: Actual system noise bandwidth (Hz)
ΔT	: Temperature difference between target and background (°C)
Δy_i	: Angular distance between scan lines
$\eta_o(\lambda_p)$	: Optical efficiency of the observer
η_{osc}	: Device overscan ratio
τ_o	: Transmittance of the optics
λ	: Wavelength of the light
Ω	: Total system noise
θ_z	: Phase angle between the MRTD target and the detectors at Nyquist frequency
σ	: Standard deviation
Γ	: Spread function width (mrad)
δ_{led}	: Angular subtense of the LED element (mrad.)
δ_s	: Sampling aperture (mrad)
δ_z	: Detector instantaneous FOV (mrad)
α_z	: Sample correlation factor along related direction
α	: Detector angular substense along horizontal direction (mrad)
β	: Detector angular substense along vertical direction (mrad)
A	: Sinusoidal vibration amplitude (mr)
A_d	: Area of a single detector (cm^2)
A_T	: Target area
ATR	: Automatic target recognition unit
b	: CRT spot size parameter
B_a	: Boost amplitude at maximum frequency (mrad.)
D	: Directional averaging operator

D_z	: Directional averaging operator
D_o	: Optics aperture diameter (cm)
DAS	: Detector angular substense (mrad.)
E_z	: Integration of the display/eye/brain in the related direction
F	: Low frequency trend
f_b	: Frequency of the maximum boost (Hz)
f_{2D}	: Frequency of the $MRTD_{2D}$
f_t	: Temporal frequency (Hz)
f_{3dB}	: 3-dB frequency of electronic roll-off (cyc/mrad)
f_{no}	: System optics f-number
f_{oc}	: Optics cut-off frequency
f_{detc}	: Detector cut-off frequency
f	: Spatial frequency (cyc/mrad)
f_x	: Horizontal spatial frequency (cyc/mrad)
f_y	: Vertical spatial frequency (cyc/mrad)
f_n	: Nyquist frequency
f_{ehp}	: Electronics 3dB frequency (Hz) for RC high pass filter
f_{elp}	: Electronics 3dB frequency (Hz) for RC low pass filter
F	: Frame rate
FOV	: Field of view (mrad)
HFOV	: Horizontal field of view (mrad)
H_{cte}	: CCD charge transfer efficiency MTF
H_{crt}	: CRT display MTF
H_{det}	: Detector modulation transfer function
H [illegible]	: Focal plane integration MTF
H_{ds}	: Detector spatial MTF
H_{disp}	: Display modulation transfer function
H_{dsh}	: Display sample and hold MTF

H_{dig} : Digital filter MTF

H_{dt} : Detector temporal MTF

H_{ehp} : Electronics low frequency response

H_{elp} : Electronics high frequency response

H_{eye} : Eye MTF

H_{eb} : Boosting MTF

H_{elect} :Electronics modulation transfer function

H_{eom} : Electro-optical multiplexor MTF

H_{ml} : Linear image motion MTF

H_{mr} : Random image motion MTF

H_{ms} : Sinusoidal image motion MTF

H_{opt} : Optics modulation transfer function

H_{odl} : Diffraction limited MTF

H_{ogb} : Geometric blur MTF

H_{ref} : Standard NETD reference filter

H_{ssp} : Sample-scene phase MTF

H_{SPF} : Spatial postfilter MTFs

H_{sys} : Total system MTF

H_{T} : Normalized fourier transform of the target

H_{TPF} : Temporal postfilter MTF

H_{pre} : Pre-sampling MTF

H_{post} : Post sampling MTF

$h_i(x,y)$:Transfer function of the imaging process

$h_r(x,y)$: Transfer function of recontruction process

$I(x,y)$: Object' s radiance in the x and y directions (scene)

$I_m(x,y)$: Image signal

$I_s(x,y;X,Y)$: Sampled image

$I_r(x,y)$: Reconstructed image

$I_{mr}(x,y)$: Ideal reconstructed image without aliasing

$I_{mar}(x,y)$: Reconstructed higher order term in aliasing effect

$\tilde{I}(f_x, f_y)$: Scene in the frequency domain

$\tilde{I}_s(f_x, f_y; X,Y)$: Sampled image in the frequency domain

k_z : Noise correction factor

k : constant, which is used to transform temperature into radiant displayed energy (watts/°C)

L : Length of a single bar of standard four bar pattern (mrad)

L_z : Spatial integration limit

$L(\lambda)$: Spectral radiance from the source (watt/ cm^2st μm)

M : Modulation

M_g : Magnification

MRTD : Minimum resolvable temperature difference (°C)

MDTD : Minimum detectable temperature difference (°C)

MTF : Modulation transfer function

N : Required cycle for detection (Johnson criterion)

N_{ccd} : Total number of charge transfers

N_{tvh} : Temporal pixel noise

N_{vh} : Fixed pixel noise

N_{tv} : Temporal row noise

N_v : Row noise

N_{th} : Temporal column noise

N_h : Column noise

N_t : Frame-to-frame noise

N_{mf} : Rms-noise output from the matched filter

NETD : Noise equivalent temperature difference (°C)

$P_s\left[\frac{x}{X}, \frac{y}{Y}\right]$: Sampling waveform

R : Input temperature / output intensity (°C/V)

R_z : Sampling rate along related direction (samp./mrad)

s	: Mean value of the all noise components
S	:Output signal
s_z	: Samples per detector angular subtense
$S_i^{'}$	: Single sided PSD at system input (watts/freq.)
S(v)	: Detector noise power spectrum
SNR	: Signal to noise ratio
T_{aspect}	: Aspect ratio of the target size
t_e	: Eye integration time (sec)
t_i	: Detector integration time (sec)
TIS	: Thermal Imaging System
U(t,v,h)	: Composite noise data set
V_n	: Noise voltage (V)
V_s	: Signal voltage (V)
v_r	: Relative image velocity (mrad/sec)
v_x	: Angular scanning velocity (mrad/sec)
VFOV	: Vertical field of view (mrad)
W	: Width of a single bar of the standard four bar pattern (mrad)

ACKNOWLEDGMENTS

The research described in this thesis was supported in part by Naval Command and Control Ocean Surveillance Center, RDT&E Division, Code 54, under NRaD project MPB45R5T25. The cooperation of the U.S. Army Night Vision and Electronic Sensors Directorate, in provision of the FLIR92 code and assistance is thankfully acknowledged.

I would like to thank Professor Ron J. Pieper and Professor Alfred W. Cooper for their guidance in the pursuit of this thesis.

I dedicate this thesis to my parents, Mete and F. Turkan Koc.

I. INTRODUCTION

A. REVIEW OF LITERATURE

Advances in thermal imaging technology have resulted in the fielding of two-dimensional array detector based imaging systems. This advancement in technology resulted in a reexamination of the applicability of the U.S. Army Night Vision Laboratory's 1975 Static Performance Model. This model was updated as FLIR90 in 1990 and finally, it was updated to FLIR92 to predict the performance of both first and second generation TISs [Ref. 9].

The minimum resolvable temperature difference (MRTD) is generally considered to be a very good performance indicator for TISs. The MRTD is experimentally measurable and it has been subject for predictive modeling. A good background reference to appreciate the significant issues in MRTD modeling is provided by Lloyd's classic text on thermal imaging systems [Ref. 1]. The MRTD model proposed in Lloyd's book is a simplified treatment of the earlier work of Ratches [Ref.4] based on the eye-brain match filter model.The Ratches MRTD model also known as the Ratches-Lawson model was based on the matched filter and synchronous integrator model [Ref. 6]. The Vortman and Bar-Lev model {ref. 5] has also been proposed to improve the MRTD predictions and compared to the MRTD models. However, questions still remain concerning the accuracy of these models [Ref.1], [Ref. 4], [Ref. 5], [Ref. 6]. The most important issues in MRTD modeling are:

1. Visual Perception

Much research has been done on this area and different theories and models have been developed. Most of this work tries to model the MTF of the eye-brain combination [Ref. 4, Ref. 8]. Recently a simple eye MTF model which assumes "a linear dependence up to a normalized peak response, at approximately 0.4 cyc./mr. , followed by a decay in response predicted by the optical in-focus OTF associated with the finite pupil size of the

eye." has been applied to MRTD modeling by Pieper [Ref. 8. P. 263]. Figure I.1 shows this bandpass MTF model for eye filter. A theory for eye and brain processing to detect sinusoidal gratings with fluctuations, which are caused by video noise, was presented by Schnitzler [Ref. 33]. The eye-brain combination is modeled as two filters by Kornfeld and Lawson [Ref.34]. The spatial-frequency filtering by the eye near to the sine-wave modulation threshold is discussed by Schnitzler [Ref.35]. The eye and brain are considered as two different filters and compared by Campbell [Ref.36].

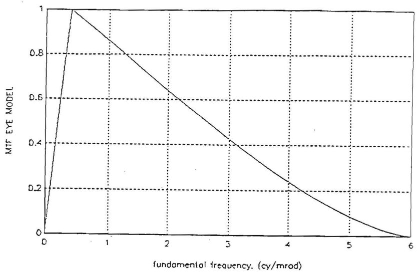

Figure I.1. A Simple Eye MTF Model (From Ref.[8])

2. Sampling

Image sampling is the processing between the continuous scene (input image), discrete sampled image signal and continuous reconstructed image. Signal conversions between them cause degradation, aliasing and blurring, in TISs. The NVEOD FLIR92 TISs Performance Model and its noise sampling effects is introduced by D' Agostino and Scott [Ref. 16]. The calculation of magnitude of the image degradation, related with

aliasing and blurring is explained by Huck, Halyo, and Park [Ref. 17]. Some methods to reduce the effects of the aliasing are proposed and the application of microscanning is explained in Watson, Muse, and Blommel, [Ref. 18]. A method to increase the sampling rate for undersampled staring systems is proposed by Chambliss, Dawson, and Borg [Ref.19]. The effects of the sensor aliasing to the target detectability is showed by Meitzler and Gerhart [Ref. 30]. The MTF of the system due to effects of the image processing is analyzed by Park, Schowengerdt, and Kaczyniski [Ref. 31].

3. Noise Characteristics

Detector noise is the dominant noise for the first generation TISs. Improvements in the TISs introduced the 3-D noise concept, because modern systems' noise show more directionality than the first generation TISs and this concept was used for FLIR92. 3-D noise methodology and its noise components are introduced by D'Agostino. 3-D noise and the usage of directional averaging operators (D operators) are defined by Webb and Bell [Ref.12]. The 3-D noise elements and the noise correction factors are explained by Scott and D'Agostino [Ref. 13]. Each of the 3-D noise components is presented by Webb [Ref. 14].

Laboratory measurements have been done objectively to compare the TISs' measured MRTD and predicted MRTD by models. The usage of automatic target recognition units to eliminate the human observer's subjectivity is being tested for different directions. Williams [Ref. 21] describes a technique to replace the observer by a CCD array camera and computer. Williams [Ref. 22] explains the requirements of objective measurement. The measurement techniques and requirements to standardize the MRTD results between the laboratories have also been given attention [Ref.23]. Recently a report has been disseminated which covers the proceedings of the 1990 NVEOD FLIR modeling workshop [Ref. 29].

B. OVERVIEW OF THE THESIS

This chapter reviews the fundamentals and basic parameters of thermal imaging systems and briefly mentions the Johnson criterion.

Chapter II defines the Ratches Model and the Lloyd Model which are applicable to first generation non-staring systems. It can be shown that these two models can be related and are equivalent to each other at low frequencies. Also, in this chapter the U.S. Army Night Vision Laboratory's FLIR92 TIS Performance Model for MRTD is compared with the Ratches and the Lloyd models.

Chapter III presents the FLIR92 TIS Performance Model under three parts. In the first part, it briefly shows the MTFs, which are used by this model. In part two, it describes the 3-D noise concept, noise applications and noise-data input groups. In part three, it defines the Minimum Resolvable Temperature Difference (MRTD) and Minimum Detectable Temperature Difference (MDTD) by using 3-D noise concept.

Chapter IV covers the effect of aliasing, which is not covered in FLIR92. It mathematically models the aliasing effect including phase artifacts due to relative shifts between the four-bar image and detector array. Computer simulations of results are shown to clarify the significance of this effect. The microscanning for reducing the aliasing effect is discussed [Ref. 18].

In Chapter V the laboratory measurements, which were done with Amber engineering AE4128 IR Imaging System and Mitsubishi Electronics IR-M500 Imager are presented. Both experimental MRTD measurements and objective measurements were done during the laboratory work.

In Chapter VI the comparisons of the FLIR92 MRTD to the measured MRTDs, which were presented in Chapter V, are presented. Also, in this chapter the limitations of the FLIR92 model are presented.

Appendix A gives the parameters of the systems, which are used in this thesis. Appendix B provides the MTF equations of FLIR92, which are listed in Chapter III.

Appendix C presents the data for experimental MRTD and objective measurements. Appendix D is short-listing outputs of the FLIR92 for Amber engineering AE4128 IR Imaging System and Mitsubishi Electronics IR-M500 Imager.

A table of symbols, which shows the symbols, acronyms and abbreviations, is included at the beginning of the thesis.

C. FUNDAMENTALS OF THERMAL IMAGING SYSTEMS

A Thermal Imaging System collects the radiated infrared energy of target and background, and changes into a visible image for an observer to detect, recognize, and identify the target. There must be a large enough temperature difference between the background and target to overcome the noise sources, nonuniform background temperature, and atmospheric attenuation. With both scanning mirrors Figure I.2 represents a serial scanning TIS [Ref. 1].

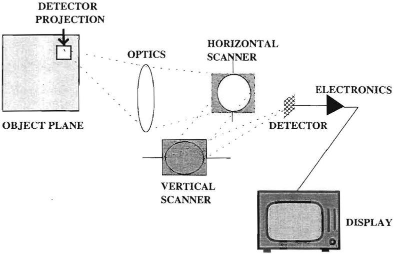

Figure I.2. A Simplified Scanning TIS (From Ref.1)

However, with only one scanner the same system would represent the common module FLIR with parallel scanning architecture [Ref. 1]. Lastly, with direct imaging on to the two dimensional detector array, i.e. no mechanical scanning, the system would represent a staring second generation design which is currently of interest [Ref. 1], [Ref. 9].

D. BASIC PARAMETERS OF THERMAL IMAGING SYSTEMS

TISs have different parameters that describe different facets of the system. In this section we are going to review definitions for Noise Equivalent Temperature Difference (NETD), Detector Angular Subtense (DAS), Optical Transfer Function (OTF), Minimum Resolvable Temperature Difference (MRTD), and Minimum Detectable Temperature Difference (MDTD).

1. NETD

This was the most used parameter to define the TIS's performance to detect small signals in noise. The following definition shows the proper way to explain this parameter: " the NETD is the blackbody target-to-background temperature difference in a standard test pattern which produces a peak-signal to rms-noise ratio (SNR) of one at the output of a reference electronic filter when the system views the test pattern" [Ref.3, p.166]

If we define the temperature difference between target and background as ΔT, signal voltage as V_s, and noise voltage as V_n, V_s/V_n can be written in the following form, by using the NETD definition [Ref. 1]:

$$\frac{V_s}{V_n} = \frac{\Delta T}{NETD} \tag{I.1}$$

From Equation (I.1) we can obtain NETD:

$$\text{NETD} = \frac{\Delta T \, V_s}{V_n} \tag{I.2}$$

As can be seen from Equations (I.1) and (I.2) when the signal voltage is equal to the noise voltage, the NETD will be equal to the temperature difference between target and background.

2. DAS

The detector collects the radiation in the limits of its Field of View (FOV). We can define FOV as Horizontal Field of View (HFOV) and Vertical Field of View (VFOV). Figure I.3 shows the DAS and FOV of a TIS. In this figure α is Horizontal DAS, β is Vertical DAS.

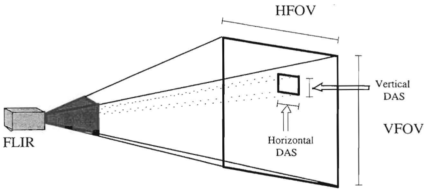

Figure I.3. Detector Angular Substense (From Ref. 1)

By using small angle approximation, DAS can be defined in the following form [Ref.2, p.82]:

$$\text{DAS}=(\text{detector size}) \,/\, (\text{effective focal length}) \tag{I.3}$$

3. OTF

OTF is the main parameter specifying the frequency response of an electro-optical system. It is composed of two parts described by [Ref. 1].

$$\mathrm{OTF} = \mathrm{MTF}\, e^{j\,\mathrm{PTF}} \tag{I.4}$$

where MTF stands for magnitude transfer function and PTF stands for phase transfer function. The MTF is also referred as the modulation transfer function which can be measured according to the following guidelines. By using Figure I.4, the modulation can be explained in the following way: "Modulation is the variation of a sinusoidal signal about its average value. " [Ref. 2, p.65]

$$\text{Modulation} = M = \frac{B\max - B\min}{B\max + B\min} = \frac{AC}{DC} \tag{I.5}$$

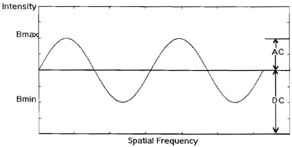

Figure I.4. Definition of Modulation

Equation (I.5) leads us to the calculation of MTF,

$$\mathrm{MTF} = \frac{M_{out}}{M_{in}} \tag{I.6}$$

Figure I.5 shows a simple block diagram of a TIS, as we can see from this figure TIS has four main blocks [Ref. 1]. The system's overall MTF is the product of the MTF values of these blocks.

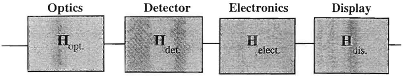

Figure I.5. Simple Block Diagram of a TIS

MTFs of this block diagram are defined as follows:

a. Optical diffraction MTF (H_{opt}):

$$H_{opt} = \frac{2}{\pi}\left[a\cos(\frac{\lambda f_x}{D_o}) - (\frac{\lambda f_x}{D_o})\sqrt{1-(\frac{\lambda f_x}{D_o})^2} \right] \quad (I.7)$$

D_o is the optics aperture diameter, λ is the wavelength of light, and f_x is the spatial frequency in the horizontal direction.

$$D_o = \lambda\, f_{oc} \quad (I.8)$$

defines an optic cutoff frequency, f_{oc}; if we insert Equation (I.8) into Equation (I.7), we can write H_{opt} in the following way:

$$H_{opt} = \frac{2}{\pi}\left[a\cos(\frac{f_x}{f_{oc}}) - (\frac{f_x}{f_{oc}})\sqrt{1-(\frac{f_x}{f_{oc}})^2} \right] \quad (I.9)$$

b. Detector spatial filter (H_{det}):

$$H_{det} = \frac{\sin(\pi f_x\ \alpha)}{\pi f_x\ \alpha} \quad (I.10)$$

Detector cutoff frequency is,

$$f_{\det c} = \frac{1}{\alpha} \tag{I.11}$$

By using Equation (I.10) and (I.11) we will have the following equation, which shows H_{det} will go to zero when $f_x = f_{detc}$.

$$H_{\det} = \sin c(\frac{f_x}{f_{\det c}}) \tag{I.12}$$

c. Electronics (H_{elect}):

As a function of temporal frequency, MTF is

$$H_{elect} = [1 + (\frac{f_t}{v_x f_{3dB}})^2]^{-0.} \tag{I.13}$$

and PTF is,

$$PTF = \arctan(-\frac{f_t}{v_x f_{3dB}}) \tag{1.14}$$

H_{elect} can be defined as a function of spatial frequency by using Equation I.15 for parallel scanning systems.

$$f_x = \frac{f_t}{v_x} \tag{I.15}$$

v_x is the angular scanning velocity. H_{elect} as a function of spatial frequency, is usually defined in this way:

$$H_{elect} = [1 + (\frac{f_x}{f_{3dB}})^2]^{-0.5} \tag{I.16}$$

and PTF is,

$$PTF = \arctan(-\frac{f_x}{f_{3dB}}) \tag{I.17}$$

d. Display (H_{dis}) :

Equation I.18 shows spot size limited display MTF, which is a gaussian distribution and b is the CRT spot size parameter in this equation. This is equivalent to assuming that the display can be described by an incoherent point spread function with a gaussian space dependence [Ref. 38].

$$H_{disp} = e^{-bf^2} \tag{I.18}$$

The equivalent of this b value is presented in Equation I. 19 [Ref. 1].

$$b = 2\pi^2 \sigma^2 \tag{I.19}$$

Typical $\frac{\sigma}{\alpha}$ value is between 0.125 and 0.5

4. MRTD

MRTD is the minimum temperature difference between the background and standard four bar pattern when four bars can be resolved by an observer. MRTD is generally considered to be a very good performance measurement for TISs. Figure I.6 shows the standard four bar pattern for four different spatial frequencies. In Figure I.6 , W, the bar width is

$$W = \frac{1}{2f_T} \tag{I.20}$$

There is a required 7:1 aspect ratio between the length and width of the bar patterns. Equation I.16 and Figure I.6 prove that spatial frequency increases as target size gets smaller, which explains why the pattern as a whole has to shrink as f_T increases. A detailed description of the MRTD by Ratches [Ref. 4] and Lloyd [Ref. 1] is going to be mentioned, in the next chapter.

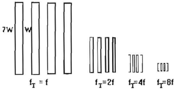

Figure I.6. Four Bar Patterns

5. MDTD

MDTD is the minimum temperature difference between background and a square target which can be detected by an observer. Figure I.7 shows this reference target

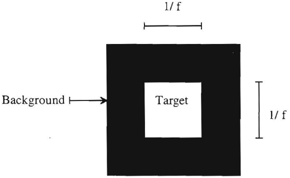

Figure I.7. Reference Square Target

The MDTD is not applied as a performance measure of TISs as frequently as the MRTD and it will not be discussed in the thesis.

E. JOHNSON CRITERION

Johnson used eight military vehicles and one observer to develop his visual discrimination methodology. During the experiment, he placed bar charts, whose length is equal to the target and width is the critical target dimension, between the observer and the targets. In classifying his laboratory results he divided the visual discrimination into the following four levels and listed the required square wave spatial frequency resolution requirement for each.

1. detection
2. orientation
3. recognition
4. identification

These discrimination levels , their meanings, and their required resolution cycles across the minimum dimension are shown in Table I.1. [Ref. 2, p.415]

Table I.1. Johnson's Results

(From Ref. 2)

DISCRIMINATION LEVEL	MEANING	CYCLES ACROSS MINIMUM DIMENSION
Detection	An object is present (object versus noise)	1.0 ± 0.025
Orientation	The object is approximately symmetrical or unsymmetrical and its orientation may be discerned (side view versus front view).	1.4 ± 0.35
Recognition	The class to which the object belongs (e.g., tank, truck, man)	4.0 ± 0.80
Identification	The object is discerned with sufficient clarity to specify the type (e.g., T-52 tank, friendly jeep)	6.4 ± 1.50

Johnson's methodology provides 50% probability of discrimination. By using the Johnson criterion, we can write an equation, which shows the connection between the target MRTD and model (four bar) MRTD [Ref. 2], as follows:

$$MRTD_{target} = \sqrt{\frac{T_{aspect}}{2N\omega}}\, MRTD \qquad (I.21)$$

ω is the aspect ratio of the target's size, the ratio of the maximum target dimension to the minimum target dimension, N is the required number of cycles for detection, T_{aspect} is the aspect ratio of the four bar pattern. In the case of interest $T_{aspect} = 7$.

F. MOTIVATION FOR THIS WORK

Recent advances in thermal imaging technology have resulted in the fielding of two-dimensional array detector based imaging systems. These "staring" designs have been labeled second-generation and are rapidly replacing existing first generation systems, some with single detectors but primarily one dimensional arrays of detectors having parallel scan type detection. It has been postulated that first generation prediction models are not applicable to second generation systems. The MRTD modeling process needed refinement in the areas of sampling, quantization noise, and array non-uniformities in order for it to be applied to second generation systems.

The purpose of this thesis is to compare the FLIR92 Performance Model for TISs to the Ratches MRTD Model and the Lloyd MRTD Model for first generation TISs and to measured data for second generation TISs.

II. FIRST GENERATION THERMAL IMAGING SYSTEMS

A. SAMPLE SYSTEM

In this chapter, the Ratches Model and the Lloyd Model are mathematical related and shown to be equivalent in the low frequency limit. A sample first generation TIS is used to compare these two models and FLIR92 Model, which is discussed in Chapter III. This sample first generation TIS is chosen from Reference 1, presented in Appendix A.

B. EYE-BRAIN MODELS

Several researchers have tried to model the MTF of the eye-brain combination. The Lloyd and the Ratches models accept the eye-brain combination as a matched filter. " The matched filter which maximizes the signal-to-noise ratio (SNR) (signal being the magnitude of the output from the matched filter and noise being the standard deviation of the noise fluctuations) at a time t_1 for the case that the noise is additive (independent of signal) and white (the power spectrum equals a constant at all frequencies). Note that for the case of a symmetrical signal and for t_1 equal to zero, the matched filter has precisely the same shape as the signal. (In general, the matched filter is the mirror image of the signal.) " [Ref.6, p.159].

FLIR92 uses a synchronous integrator model for MRTD prediction and matched filter concept for MDTD prediction. The synchronous integrator model can be defined in the following way: " the eye/brain combination will integrate over the entire area of an image even though the image has been smeared out over a large distance by finite apertures. In the formulation for signal, the integration limits are plus or minus infinity although as a practical matter the effective distance is usually much smaller because signal integrated in the low-amplitude tails of a blurred image in a real imaging system

increases only very slowly with increase in integration distance from the image center or core " [Ref. 6, p. 159]. The matched filter concept was mentioned in Chapter II.

The Visibility Model [Ref. 8] uses an MTF_{eye} based on an approximate sine wave response (SWR) model. This eye MTF model was mentioned in Chapter I and Figure I.1 shows the MTF eye model as a band pass filter, which compares well with cited human eye responses, after conversions to cycles/degree.

C. NETD

Reference 6 derives and presents the NETD in the following way:

$$\mathrm{NETD} = \frac{4 f_{no}^2 (\Delta f_n)^{0.5}}{\pi (A_d)^{0.5} \int_0^\infty \eta_o(\lambda) \frac{\delta L_\lambda}{\delta T} D^*(\lambda) d\lambda} \quad [^\circ C] \tag{II.1}$$

Δf_n is noise equivalent electrical bandwidth, A_d is the area of a single detector, $\eta_o(\lambda_p)$ is the optical efficiency of the lens, and L_λ is spectral radiance from the source, f_{no} is the ratio of the focal length of the collecting lens to the diameter of collecting lens. For calculation by hand, $\int \frac{\delta L_\lambda}{\delta T}$ is given 5.2 10^{-6}, between 3.2 and 4.8μm, and 7.4 10^{-5}, between 8 and 13μm. Reference 1 derives and uses some approximations to give a simple NETD equation, which is shown in Equation (II.2):

$$\mathrm{NETD} = \frac{\pi \sqrt{a b \Delta f_R}}{\alpha \beta A_o \tau_o D^*(\lambda_p) \frac{\Delta W}{\Delta T}} \tag{II.2}$$

In this equation a and b are detector dimensions, A_o area of the optics, τ_o is optical transmission,α and β are detector angular subtenses, $\frac{\Delta w}{\Delta T}$ is 1.48 10^{-4} between 8 and 11.5μm.

D. MRTD

The Ratches MRTD Model and the Lloyd MRTD Model define the MRTD value in the following ways:

The Ratches MRTD,

$$MRTD_R = \frac{\frac{\pi^2}{8} SNR_{th} NETD}{L H_{sys}(f_x) \int_{-\infty}^{\infty} H_T^2(f_y) H_{sys}^2(f_y) df_y} \left(\frac{v_x \Delta y_i}{\Delta f_n F_r t_e}\right)^{0.5} \times \tag{II.3}$$
$$\left[\int_{-\infty}^{\infty} \int_0^{\infty} \frac{S_i'(f_x)}{S_i'(f_T)} H_{elect}^2(f_x) H_{disp}^2(f_x, f_y) H_w^2(f_x) H_T^2(f_y) H_{sys}^2(f_y) df_x df_y\right]^{0.5}$$

The Lloyd MRTD,

$$MRTD_L = \frac{0.66 SNR_{th} NETD f_x}{(\Delta f_r)^{0.5} H(f_x)} \left(\frac{\alpha \beta}{\dot{F} t_e \tau_d}\right)^{0.5} \tag{II.4}$$

Target temporal frequency f_t can be changed to the target spatial frequency by using Equation (II.5) for first generation parallel scanning systems; its usage has limitations for second generation systems.

$$f_t = \frac{\alpha}{\tau_d} f_T \tag{II.5}$$

If these two MRTD models are compared to each other, it is seen that the Ratches model defined $\frac{\alpha}{\tau_d} = v_x$ and $\frac{7}{2 f_T} = L$. By using these corresponding terms in the Equation (II.3),

it can be rewritten as follows:

$$MRTD_R = \frac{\left(\frac{\pi^2}{8}\right) SNR_{th} NETD\, f_T \sqrt{\frac{2}{7}} \sqrt{\frac{2}{7}}}{H_{sys}(f_x) \int_{-\infty}^{\infty} H^2_{sys}(f_y) H^2_T(f_y)\, df_y} \left(\frac{\alpha\beta}{\tau_d\, t_e\, F \Delta f_r} \right)^{0.5} \times \tag{II.6}$$

$$\left[\int_{-\infty}^{\infty} \int_0^{\infty} \frac{S'_i(f_x)}{S'_i(f_T)} H^2_{elect}(f_x) H^2_{disp}(f_x, f_y) H^2_w(f_x) H^2_T(f_y) H^2_{sys}(f_y)\, df_x\, df_y\right]^{0.5}$$

Substituting related terms in Equation (II.6) with Equation (II.4) gives,

$$MRTD_R = MRTD_L \sqrt{\frac{2}{7}} \frac{1}{\int_{-\infty}^{\infty} H^2_{sys}(f_y) H^2_T(f_y)\, df_y} \times \tag{II.7}$$

$$\left[\int_{-\infty}^{\infty} \int_0^{\infty} \frac{S'_i(f_x)}{S'_i(f_T)} H^2_{elect}(f_x) H^2_{disp}(f_x, f_y) H^2_w(f_x) H^2_T(f_y) H^2_{sys}(f_y)\, df_x\, df_y\right]^{0.5}$$

Length of the four bar pattern is seven times its width,

$$\sqrt{\frac{2}{7}} = \sqrt{\frac{2W}{L}} \tag{II.8}$$

S:

$$MRTD_R = MRTD_L \left(\frac{2W}{L}\right)^{0.5} \frac{1}{\int_{-\infty}^{\infty} H^2_{sys}(f_y) H^2_T(f_y)\, df_y} \times \tag{II.9}$$

$$\left[\int_{-\infty}^{\infty} \int_0^{\infty} \frac{S'_i(f_x)}{S'_i(f_T)} H^2_{elect}(f_x) H^2_{disp}(f_x, f_y) H^2_w(f_x) H^2_T(f_y) H^2_{sys}(f_y)\, df_x\, df_y]\right]^{0.5}$$

Equation (II.9) shows that there is a conversion factor between the $MRTD_R$ and $MRTD_L$

as proposed by Reference 8. By using this conversion factor, χ, it can be shown as Equation (II.11):

$$\chi(f_T) = \left(\frac{2W}{L}\right)^{0.5} \frac{\left(\int_0^{\infty} H^2_{elect}(f_x)\, H^2_w(f_x)\, H^2_{disp}(f_x)\, df_x\right)^{0.5}}{\int_{-\infty}^{\infty} H^2_T(f_y)\, H^2_{sys}(f_y)\, df_y} \qquad \text{(II.10)}$$

By using (II.10),

$$MRTD_R = MRTD_L\, \chi(f_T) \qquad \text{(II.11)}$$

To show these MRTD models converge as spatial frequency goes to zero, low frequency approximations are used. These approximations are as follows [Ref.6]:

$$\int_{-\infty}^{\infty} H^2_T(f_y)\, H^2_{sys}(f_y) H^2_{disp}(f_y) df_y \approx \frac{1}{L} \qquad \text{(II.12)}$$

$$\int_{-\infty}^{\infty} H^2_T(f_y)\, H^2_{sys}(f_y) df_y \approx \frac{1}{L} \qquad \text{(II.13)}$$

$$\int_0^{\infty} \frac{S_i'(f_x)}{S_i'(f_T)} H^2_{elect}(f_x)\, H^2_{disp}(f_x)\, H^2_w(f_x) df_x \approx \frac{1}{2W} \qquad \text{(II.14)}$$

When these approximation terms are applied to the Equation (II.9),

$$MRTD_R = MRTD_L \qquad \text{(II.15)}$$

which shows that at low frequencies these two models are equal to each other. Equation (II.4) shows as spatial frequency goes to zero $MRTD_L$ goes to zero, so $MRTD_R$ goes to zero.

FLIR92 model is covered in the next chapter and Equation (III.19) shows that FLIR92 MRTD goes to zero when spatial frequency goes to zero.

The Visibility Model agrees with the Static Performance Model except at very low and very high frequencies. This model assumes that the bar pattern acts like a step function in the zero frequency limit. The low frequency limit, accepted by this model, corresponds to a minimum system degraded temperature difference, which is enough to be recognized by observer or sensor. This model proposes that there is a critical response, ΔT_{sc}, below which the four bar target recognition is not possible. This value is the response amplitude related with the MRTD of the measurement. A four bar frequency response can be written in the following form:

$$\alpha_r = \frac{\Delta T_{sc}}{MRTD} \tag{II.16}$$

By using Equation (II.16), the MRTD zero frequency limit relation can be shown as follows:

$$MRTD(f = 0) = \frac{\Delta T_{sc}}{\alpha_r(f=0)} \tag{II.17}$$

In this part, the sample system which is given in Appendix A was used to compare FLIR92 TIS Performance Model to the Ratches Model and the Lloyd Model for first generation TISs. Figure II.1. shows output from the Ratches Model and Lloyd Model; it can be seen that $MRTD_L$ value is more optimistic than $MRTD_R$. Figure II.2. compares the Ratches Model, Lloyd Model, and FLIR92 Model. Figure II.3 is the logarithmic presentation of Figure II.2. The Ratches Static Performance Model was developed into FLIR90 and finally FLIR92. These figures show that between $MRTD_R$ and FLIR92 MRTD values there is difference; FLIR92 is more optimistic, and FLIR92 values are closer to the $MRTD_L$.

As shown the Ratches and the Lloyd MRTD Models go to zero when spatial frequency goes to zero Since FLIR92 MRTD output list starts from 0.05 cyc/mrad, the

low frequency MRTD limit for FLIR92 MRTD can not be established from the data generated. However, Equation (III.19) shows it goes to zero for zero spatial frequency, and for this sample system it determines the Nyquist frequency as 0.5 cyc/mrad, which is MRTD values are not calculated after this frequency. The FLIR92 output list gives Horizontal MRTD, Vertical MRTD, and 2D MRTD. In Figure II.2 and II.3 the 2D MRTD was plotted.

$MRTD_R$ and $MRTD_L$ are shown plotted and the logical flowchart of these models is given in Figure II.4

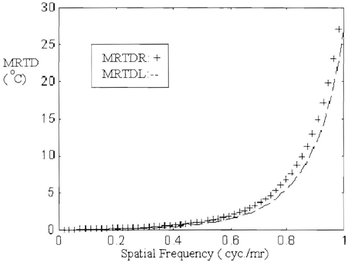

Figure II.1 Ratches and Lloyd MRTD Models

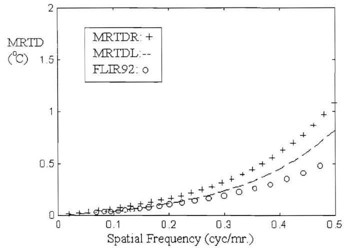

Figure II.2. Ratches, Lloyd, and FLIR92 MRTD Models

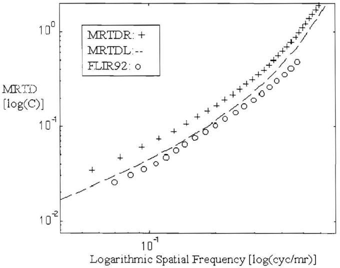

Figure II.3. Logarithmic Presentation of MRTD Models

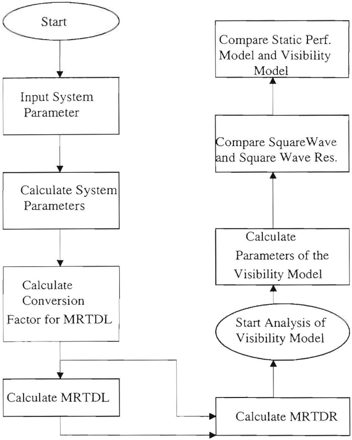

Figure II.4. Visibility Model Logic Flowchart

III. U.S. ARMY NVSED FLIR92 TIS PERFORMANCE MODEL

U.S. Army Night Vision Laboratory developed the 1975 Night Vision Laboratory Static Performance Model for first generation serial and parallel scanning TISs. This model was one dimensional and did not take account of noise sources, except for random noise, and effects of sampling. Because of the improvement in TISs, second generation systems replaced first generation systems, and this model couldn't predict exactly the second generation TISs' performance. In 1990, C^2 NVEO developed the FLIR90 TISs model to cover the different noise sources and sampling effects. This model was updated as the FLIR92 TIS Performance Model in 1992. This new model predicts NETD, MRTD, and MDTD [Ref.2] [Ref. 9]

This model can be defined in the following way: " FLIR92 models parallel scan, and staring thermal imagers that operate in the mid and far infrared spectral bands. The model can only be used for thermal imagers and is not capable of predicting performance for any other class of electro-optical sensor. The model doesn't predict target acquisition/ discrimination range performance." [Ref. 9, p. ARG-1]

In this chapter, FLIR92 will be covered under three headings:

a. MTFs

b. Noise

c. MRTD and MDTD

A. MTFs

FLIR92 calculates MTFs in three main groups. The product of these groups gives us the system's overall MTF. MTFs, which are calculated by this model, are as follows:

1. Prefilter MTFs

    a. Optics MTFs

(1) Diffraction-limited MTF

(2) Geometric Blur MTF

(3) Measured Optics MTF

b. Detector Spatial MTF

c. Focal Plane Array Integration Time

d. Sample-scene Phase MTF

e. Image Motion MTFs

(1) Linear Image Motion MTF

(2) Random Image Motion MTF

(3) Sinusoidal Image Motion MTF

f. Spare Filter MTF

2. Temporal Postfilter MTFs

a. Detector Temporal MTF

b. Electronics Low Frequency Response

c. Electronics High Frequency Response

d. Boosting MTF

e. Spare Temporal Postfilter MTF

3. Spatial Postfilter MTFs

a. Electro-optical Multiplexor MTF

b. Digital Filter MTF

c. Display MTF

(1) CRT Display MTF

d. CCD Charge Transfer Efficiency MTF

e. Display Sample and Hold MTF

f. Eye MTF

(1) Non-limiting Eye MTF

(2) Limiting Eye MTF

g. Spare Spatial Postfilter MTFs

Equations for these MTFs are given in Appendix B. The short listing output of the FLIR92 gives MTF values of three main groups; the long listing output of FLIR92 gives all MTF values under the three main groups.

B. NOISE

NETD was used to predict the system performance for first generation TISs. When second generation TISs began to be used, it was noticed that system performance couldn't exactly be predicted by using NETD, because these advanced systems use complex signal processing techniques which cause new types of noises and these noises can be defined in coordinate system by averaging them in specific directions [Ref. 14]. These noises affect the calculation of MRTD using the performance prediction models which were used for first generation systems. That does not mean that first generation systems do not have directional noise, but detector noise is the dominant noise, affecting the calculation of MRTD for these systems.

FLIR92 model uses the 3-D noise concept for scanning and staring sensors. Dimensions of this 3-D noise are t, frame number, v, row number, and h, column number as seen in Figure III.1.

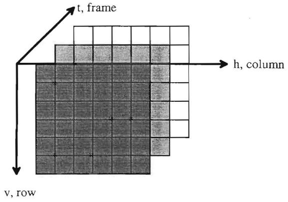

Figure III.1. 3-D Noise Directions (After Ref.[11])

There are totally seven noise components in these three directions, but the grand mean of all these seven noise components can be treated as an eighth noise component. In the following Table III.1, these eight noise components are shown.

Direction	vh	v	h	-
t	N_{tvh}	N_{tv}	N_{th}	N_t
-	N_{vh}	N_v	N_h	s

Table III.1. 3-D Noise Components

The total system noise U(t,v,h) can be written as [Ref. 9]

$$U(t,v,h)=N_{tvh}+N_{tv}+N_{th}+N_{vh}+N_v+N_h+N_t+s \qquad \text{(III.1)}$$

where all terms except the grand mean represent fluctuations about a mean of zero.

1. Directional Averaging Operators (D Operators)

3-D Noise components are random fluctuating values about the mean value in the direction to which they relate. That's why we need to average these values. Variations can be integrated out by using D operators in the needed directions. Basically, these D operators cancel the unwanted noise effect components. The processing definitions of these operators can be seen in Table III.2.

Noise Term	3-D Process Definition
N_{tvh}	$[(1-D_t)(1-D_v)(1-D_h)]\{U(t,v,h)\}$
N_{vh}	$[D_t(1-D_v)(1-D_h)]\{U(t,v,h)\}$
N_{tv}	$[(1-D_t)(1-D_v)D_h]\{U(t,v,h)\}$
N_v	$[D_t(1-D_v)D_h]\{U(t,v,h)\}$
N_{th}	$[(1-D_t)D_v(1-D_h)]\{U(t,v,h)\}$
N_h	$[D_tD_v(1-D_h)]\{U(t,v,h)\}$
N_t	$[(1-D_t)D_vD_h]\{U(t,v,h)\}$
s	$[D_tD_vD_h]\{U(t,v,h)\}$

Table III.2. Process Definition of 3-D Operators (After Ref.[12])

At this point an illustration of the use of the D operators is presented. If N_{tv} is to be calculated, $(1-D_t)$, $(1-D_v)$, and D_h are used since we want to cancel the noise components only in the h (horizontal) direction. If these operators, $(1-D_t)$, $(1-D_v)$, and D_h are multiplied with the system total noise U(t,v,h), it will give the desired N_{tv} component. The following steps are provided for justification of the process. Which is illustrated in Figure III.3 [Ref. 11]

a. The D_t operator has 0 value for operation on all noises in the temporal variation. To produce the $(1-D_t)$ operator it is necessary to subtract all noise values of D_t from 1.

b. The D_v operator has 0 value for operation on all noises in the vertical variation. To produce $(1-D_v)$ operator it is necessary to subtract all noise values of D_v from 1.

c. The D_h operator has 0 value for operation on all the noises in the horizontal variation.

d. Multiply the same noise components of the $(1-D_t)$, $(1-D_v)$, and D_h.

e. The result of the step-d gives only N_{tv} noise component and cancels the other noise components. Which demonstrates that the validity of the N_{tv} row of Table III.2.

Another approach to the usage of D operators has been suggested [Ref. 12]. This approach is described briefly in Appendix B.

D_t (a) →

Ntvh	Ntv	Nth	Nt
0	0	0	0
Nvh	Nv	Nh	s
1	1	1	1

$1\text{-}D_t$

Ntvh	Ntv	Nth	Nt
1	1	1	1
Nvh	Nv	Nh	s
0	0	0	0

(d) X

D_v (b) →

Ntvh	Ntv	Nth	Nt
0	0	1	1
Nvh	Nv	Nh	s
0	0	1	1

$1\text{-}D_v$

Ntvh	Ntv	Nth	Nt
1	1	0	0
Nvh	Nv	Nh	s
1	1	0	0

(d) X

(c) D_h

Ntvh	Ntv	Nth	Nt
0	1	0	1
Nvh	Nv	Nh	s
0	1	0	1

↓

(e)

Ntvh	Ntv	Nth	Nt
0	1	0	0
Nvh	Nv	Nh	s
0	0	0	0

Figure III.2. The Processing of D Operators: Calculation of N_{tv}, the Temporal Vertical Noise Component

2. Analysis

Another step that must be taken in the 3-D noise application is the calculation of the standard deviation of the noise components expressed in degrees. The values of these standard deviations are represented by σ_{xyz} (where xyz is the related direction). For example calculation of the σ_{tvh} is shown by Equation III.2.

$$\sigma_{tvh} = (\mathrm{stddev}(N_{tvh}(1 - F)))R \qquad \text{(III.2)}$$

where the average standard deviation is performed in this case over directions t, v, h along pixel streams. In this equation, F is the low frequency trend, which is low frequency fixed pattern noise [Ref. 14], and R is the ratio of input temperature to the output intensity measured in (°C/Volt). High frequency variations have the biggest effect on the system performance predictions so it is necessary to remove the low frequency trend in spatial noise. By removing the low frequency trend, high frequency variations will be made dominant in the direction of the noise component. The values of the other noise components can be calculated by changing Equation III.2 for their directions. For calculation of the s-component, we don't need any trend subtraction or standard deviation; we multiply it by ratio of input temperature and output intensity. Table III.3 shows 3-D noise components and their sources [Ref. 2, p.386]. The following equation shows the relation between the classic NETD and 3-D noise component [Ref. 9]:

$$\sigma_{tvh} = \mathrm{NETD} \times \sqrt{\frac{\Delta f_p}{\Delta f_n}} = \frac{4 f_{no}^2 \sqrt{\Delta f_p}}{\pi \tau_o \sqrt{A_d} \left(\int_{\lambda_1}^{\lambda_2} D^*(\lambda, 300) \frac{\delta W(\lambda)}{\delta T_{300}} d\lambda \right)} \qquad \text{(III.3)}$$

which follows from the fact that σ_{tvh} is a composite measure of noise for all three directions. Δf_p is actual system noise bandwidth associated with the system electronics prior to display; for scanning and staring systems this bandwidth can be shown in the following way:

3D Noise Component	Description	Serial Scan	Parallel Scan	Staring Array
σ_{tvh}	Random 3-D noise	Random and 1/f noise	Random and 1/f noise	Random
σ_{vh}	Spatial noise that does not change from frame-to-frame	-	-	FPN
σ_{th}	Variations in column averages that change from frame-to-frame (rain)	Microphonics	Microphonics	Readout noise
σ_{tv}	Variations in row averages that change from frame-to-frame (streaking)	1/f noise	Transients (flashing detectors), 1/f noise	Readout noise
σ_{v}	Variations in row averages that are fixed in time (horizontal lines or bands)	Line-to-line interpolation	Detector gain/level variations, line-to-line interpolation	Readout noise, line-to-line interpolation
σ_{h}	Variations in column averages that are fixed in time (vertical lines)	Shading	Shading	Readout noise
σ_{t}	Frame-to-frame intensity variations (flicker)	Frame processing	Frame processing	Frame processing

Table III.3. Seven Noise Components of The 3-D Noise Model [Reference 2]

for scanning systems,

$$\Delta f_p = \int_0^\infty S(v) H_{TPF}^2(v) dv \tag{III.4}$$

for staring systems,

$$\Delta f_p = \int_0^\infty S(v) \left(\frac{\sin(\pi v t_i)}{\pi v t_i} \right) dv \tag{III.5}$$

where t_i is the focal plane array integration time, S(v) is normalized detector noise power spectrum and H_{TPF} is the temporal post filter defined in Appendix B. Δf_n is the equivalent noise bandwidth for the NETD and can be defined as:

$$\Delta f_n = \int_0^\infty S(v) H_{ref}^2(v) dv \tag{III.6}$$

where H_{ref}^2 is the standard NETD reference filter [Ref. 1].

The total system noise, generated from the statistically independent standard deviation noise components, σ_{xyz}, can be written as [Ref. 13, p. ARG-33]:

$$\Omega = \left[\sigma_{tvh}^2 + \sigma_{th}^2 + \sigma_{tv}^2 + \sigma_{vh}^2 + \sigma_h^2 + \sigma_v^2 + \sigma_t^2 \right]^{0.5} \tag{III.7}$$

Total system noise in horizontal and vertical directions can be seen in the following Equations (III.8) and (III.9):

for the horizontal direction,

$$\Omega_h = \left[\sigma_{tvh}^2 E_t E_v(f) E_h(f) + \sigma_{vh}^2 E_v(f) E_h(f) + \sigma_{th}^2 E_t E_h(f) + \sigma_h^2 E_h(f) \right]^{0.5} \tag{III.8}$$

for the vertical direction,

$$\Omega_v = \left[\sigma_{tvh}^2 E_t E_v(f) E_h(f) + \sigma_{vh}^2 E_v(f) E_h(f) + \sigma_{tv}^2 E_t E_v(f) + \sigma_v^2 E_v(f)\right]^{0.5} \qquad \text{(III.9)}$$

E_t, $E_v(f)$, and $E_h(f)$ are the integration factors of the display/eye/brain in the related directions. These integration factors are [Ref. 13]:

The temporal integration factor is,

$$E_t \approx \frac{\alpha_t}{F_r\, t_e} \qquad \text{(III.10)}$$

where F_r is the system frame rate, t_e is the eye integration time, and α_t is the sample correlation factor. α_t is usually taken to be 1.

The vertical integration factor is,

$$E_v(f) \approx \frac{\alpha_v}{R_v\, L_v(f)} \qquad \text{(III.11)}$$

where R_v is the vertical sampling rate (samp./mrad), $L_v(f)$ is the vertical spatial integration limit, which in this approximate form is the vertical dimension of the MRTD bar target, and α_v is the vertical sample correlation factor [Ref. 9].

The horizontal integration factor is,

$$E_h(f) \approx \frac{\alpha_h}{R_h\, L_h(f)} \qquad \text{(III.12)}$$

where R_h is the horizontal sampling rate (samp./mrad), $L_h(f)$ is the horizontal spatial integration limit, which in this approximation is the horizontal dimension of the MRTD bar target, and α_h is horizontal sample correlation factor. For staring systems α_v and σ_h

are usually taken to be one [Ref. 9].

3. Noise-Data Input Groups

There are three different noise-data input groups in FLIR92. By using any one of these groups, desired noise information can be entered into the model. These noise-data groups are:

a. 3-D Noise Default: If we don't specifically assign noise values, FLIR92 model assigns default values as a percentage of σ_{tvh} for the system's critical noise components, which are shown in Table III.4. Moderate noise level, for scanning systems, and low noise level, for staring systems, are recommended and used as default values.

b. 3-D Noise Measurements: This data group is used to enter the exact 3-D noise values.

c. 3-D Noise Estimates: This data group is used to enter the estimated 3-D noise values as a percentage of σ_{tvh}.

System	Noise Component	No Noise Default	Low Noise Default	Moderate Noise Default	High Noise Default
Scanning	σ_{tv}, σ_{v}	0	$0.25 \times \sigma_{tvh}$	$0.75 \times \sigma_{tvh}$	$1.0 \times \sigma_{tvh}$
Staring	σ_{vh}	0	$0.40 \times \sigma_{tvh}$	-	-

Table III.4. FLIR92 3-D Noise Default Values

C. MRTD AND MDTD

FLIR92 uses synchronous integrator model for MRTD prediction and matched filter concept for MDTD prediction. Synchronous integrator model and matched filter concept were mentioned in Chapter II.

FLIR92 corresponding to the direction of the standard four bar pattern calculates the horizontal and the vertical MRTD. Horizontal and vertical orientations of the four bar

pattern are shown in Figure III.3. Using these two MRTD values, FLIR92 calculates the $MRTD_{2D}$, for which the spatial frequency is defined by Equation (III.13).

$$f_{2D} = \sqrt{f_x \cdot f_y} \qquad \text{(III.13)}$$

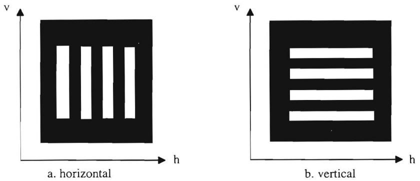

Figure III.3. MRTD Target Patterns (From Ref. 9, p. ARG-2)

MRTD and MDTD are described by the following equations [Ref. 9]:

$$MRTD_z(f) = \frac{\pi^2 SNR_{th}\,\Omega_z}{H_{sysz}(f)} \qquad \text{(III.14)}$$

where the z subscript refers to the horizontal or vertical direction as required and MDTD is

$$MDTD(f) = \frac{SNR_{th}\,\sigma_{tvh}\,\Omega}{A_T Q_h(f) Q_v(f)} \qquad \text{(III.15)}$$

We can write the total system noise, Equation (III.8) and (III.9), in the form

$$\Omega_z = \sigma_{tvh}\, k_z\, [E_t\, E_h(f)\, E_V(f)]^{0.5} \qquad \text{(III.16)}$$

where k_z is the correction factor in the horizontal or vertical direction. Using Equations (III.14), (III.15), and (III.16), MRTD and MDTD can be rewritten as follows:

$$MRTD_z(f) = \left(\frac{\pi^2 SNR_{th}\,\sigma_{tvh}\,k_z(f)}{H_{sys_z}(f)}\right)[E_t\,E_h(f)\,E_v(f)]^{0.5} \qquad \text{(III.17)}$$

If horizontal MRTD for scanning systems is written by using the exact equations of the display/eye/brain integration, [Ref.9,p.ARG-39] instead of using any approximation, it gives the following equation:

$$MRTD_h = \frac{\frac{\pi^2}{8} SNR_{th}\,\sigma_{tvh}\,k_h(f)}{H_{sys}(f)}\left[\frac{1}{F_r t_e}\left(\frac{v_x}{\Delta f_n}\int_0^{\infty} S(v)H_{nf}^2(v)\left(\frac{\sin\left(\frac{\pi v}{2f}\right)}{\frac{\pi v}{2f}}\right)^2 dv\right)\right. \qquad \text{(III.18)}$$

$$\left.\times\left(\frac{IFOV}{s_v}\int_0^{\infty} H_{nf}^2(v)\left(\frac{\sin\left(\frac{7\pi v}{2f}\right)}{\frac{7\pi v}{2f}}\right)^2 dv\right)\right]^{0.5}$$

By choosing one of the integrals in (III.18), i.e. first integral, it can be shown that FLIR92 MRTD value goes to zero. If $\frac{\pi v}{2f}$ is defined as x, the first integral can be written as follows:

$$\frac{v_x}{\Delta f_n}\int_0^{\infty} S(v)H_{nf}(v)\left(\frac{\sin\left(\frac{\pi v}{2f}\right)}{\frac{\pi v}{2f}}\right)^2 dv = \frac{v_x}{\Delta f_n}\frac{2f}{\pi}\int_0^{\infty} S\left(\frac{2xf}{\pi}\right)H_{nf}\left(\frac{2xf}{\pi}\right)\left(\frac{\sin(x)}{x}\right)^2 dx \qquad \text{(III.19)}$$

Equation (III.19) proves that FLIR92 MRTD is equal to zero when spatial frequency is equal to zero. MDTD value for FLIR92 is,

$$MDTD(f) = \left(\frac{SNR_{th}\,\sigma_{tvh}\,k_{MDTD}(f)}{A_T Q_h(f) Q_v(f)}\right)[E_t\,E_h(f)\,E_v(f)]^{0.5} \qquad \text{(III.20)}$$

where $Q_h(f)$ and $Q_v(f)$ are given in following equation:

$$Q_z(f) = \int_{-\infty}^{\infty} H^2_{sys_z}(v) \left(\frac{\sin\left(\frac{\pi v}{f}\right)}{\frac{\pi v}{f}} \right)^2 dv \tag{III.21}$$

By using Equation (III.8), (III.9), and (III.16) correction factor, $k_z(f)$, can be written :

for the horizontal direction as

$$k_h(f) = \left[1 + \left(\frac{\sigma_{vh}}{\sigma_{tvh}} \right)^2 \frac{1}{E_t} + \left(\frac{\sigma_{th}}{\sigma_{tvh}} \right)^2 \frac{1}{E_v(f)} + \left(\frac{\sigma_h}{\sigma_{tvh}} \right)^2 \frac{1}{E_t\, E_v(f)} \right]^{0.5} \tag{III.22}$$

for vertical direction as

$$k_v(f) = \left[1 + \left(\frac{\sigma_{vh}}{\sigma_{tvh}} \right)^2 \frac{1}{E_t} + \left(\frac{\sigma_{tv}}{\sigma_{tvh}} \right)^2 \frac{1}{E_h(f)} + \left(\frac{\sigma_v}{\sigma_{tvh}} \right)^2 \frac{1}{E_t\, E_h(f)} \right]^{0.5} \tag{III.23}$$

and for the MDTD as

$$k_{MDTD} = [\, 1 + \left(\frac{\sigma_{vh}}{\sigma_{tvh}} \right)^2 \frac{1}{E_t} + \left(\frac{\sigma_{th}}{\sigma_{tvh}} \right)^2 \frac{1}{E_v(f)} + \left(\frac{\sigma_h}{\sigma_{tvh}} \right)^2 \frac{1}{E_t\, E_v(f)} + \tag{III.24}$$

$$\left(\frac{\sigma_{tv}}{\sigma_{tvh}} \right)^2 \frac{1}{E_h(f)} + \left(\frac{\sigma_v}{\sigma_{tvh}} \right)^2 \frac{1}{E_t\, E_h(f)} \,]^{0.5}$$

If it is assumed that the recommended default values, i.e. moderate noise for scanning systems and low noise for staring systems, are used from Table III.4, then the correction factors can be simplified to the following forms:

for scanning systems,

$$k_h(f) = 1 \tag{III.25}$$

and,

$$k_v(f) = k_{MDTD}(f) = \left[1 + (0.5625)\frac{R_h L_h(f)}{\alpha_h} + (0.5625)\frac{F_r t_e R_h L_h(f)}{\alpha_t \alpha_h}\right]^{0.5} \tag{III.26}$$

for staring systems,

$$k_h(f) = k_v(f) = k_{MDTD}(f) = \left[1 + (0.16)\frac{F_r t_e}{\alpha_t}\right]^{0.5} \tag{III.27}$$

These correction factors can be inserted in to the MRTD and MDTD equations, (III.17) and (III.18).

IV. ALIASING

Analog-to-digital and digital-to-analog signal conversions cause degradation in TISs. Aliasing and blurring contribute significantly to this degradation. Aliasing is created by sampling at less than the Nyquist frequency. Blurring, a term commonly used for images, is generated when the image is spatially low pass filtered [Ref. 38]. In this chapter, aliasing models relevant to electronic imaging will be covered. Figure IV.1 shows a block diagram of a sampled TIS. This model will be described in more detail in the next section.

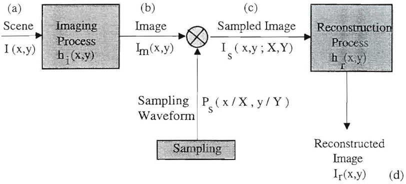

Figure IV.1. Block Diagram of a Sampled TIS (After Ref. [17])

A. MODEL

The processes illustrated in Figure IV.1 are described in the space domain and frequency domain by following steps [Ref. 17] :

1. In the space domain

a. Scene is the object's radiance distribution in the x and y directions: $I(x,y)$

b. Imaging process is the convolution of the input signal, $I(x,y)$, with the transfer function of the imaging process, $h_i(x,y)$. This process gives the image:

$$I_m = I(x,y) * h_i(x,y) \tag{IV.1}$$

where * indicates convolution.

c. Multiplication of the image with the sampling waveform gives the sampled image:

$$I_s(x,y;X,Y) = I_m(x,y)\, P_s\left[\left(\frac{x}{X}\right),\left(\frac{y}{Y}\right)\right] \tag{IV.2}$$

where X and Y are the spatial periods for periodic sampling in the x and y directions. If $P_s\left(\frac{x}{X},\frac{y}{Y}\right)$ is an infinite array of impulses the sampling process is "ideal".

d. The reconstruction process is the convolution of the sampled image signal, I_s, with the transfer function of the reconstruction process, $h_r(x,y)$:

$$I_r(x,y) = I_s(x,y;X,Y) * h_r(x,y) \tag{IV.3}$$

2. In the frequency domain, these steps (a, b, c, d) can be expressed by using

Fourier transforms. The two dimensional Fourier transform operator can be defined [Ref.38]:

$$\mathcal{F}\{G(x,y)\} = \int_{-\infty}^{\infty}\int_{-\infty}^{\infty} G(x,y)\, e^{-j2\pi x f_x}\, e^{-j2\pi y f_y} dx\, dy = \tilde{G}(f_x, f_y) \quad \text{(IV.4)}$$

where f_x and f_y are the spatial frequencies. The inverse transform is at the same mathematical form except the complex exponentials are complex conjugated. This relation can also define the one dimensional transform. If G(x,y) separates, i.e. G(x,y)= G(x)G(y) then $\mathcal{F}\{G(x,y)\} = \mathcal{F}_{1D}\{G(x)\}\ \mathcal{F}_{1D}\{G(y)\}$.

a. The Fourier transform of the scene is:

$$\tilde{I}(f_x, f_y) = \mathcal{F}\{\, I(x,y)\,\} \quad \text{(IV.5)}$$

b. The image spectrum is obtained by taking the Fourier transform of the image signal $I_{m'}(x,y)$. Application of the convolution theorem [Ref. 38] leads to:

$$\tilde{I}_m(f_x, f_y) = \tilde{I}(f_x, f_y) H_i(f_x, f_y) \quad \text{(IV.6)}$$

c. The spectrum of the ideal sampling waveform [Ref. 17] is:

$$\tilde{P}_s(Xf_x, Yf_y) = \frac{1}{XY} \sum_{m=-\infty}^{\infty} \sum_{n=-\infty}^{\infty} \delta\left[\left(f_x - \frac{m}{X}\right), \left(f_y - \frac{n}{Y}\right)\right] \quad \text{(IV.7)}$$

where m and n are indices that identify where sampling occurs.It is worth noting that the ideal case can be applied to nonideal sampling, i.e. sampling with pulses instead of impulses, by prefiltering the image spectrum $\tilde{I}(f_x, f_y)$ with a lowpass transfer function associated with the window process of the detector [Ref. 1. p. 376].

d. The ideal sampled image is,

$$\tilde{I}_s(f_x, f_y; X, Y) = \tilde{I}_m(f_x, f_y) * \tilde{P}_s(Xf_x, Yf_y) \tag{IV.8}$$

By using Equation (IV.7), the sampled image spectrum can be expressed as an infinite sum of terms as shown.

$$\tilde{I}_s(f_x, f_y; X, Y) = \sum_{m=-\infty}^{\infty} \sum_{n=-\infty}^{\infty} \tilde{I}_m\left[\left(f_x - \frac{m}{X}\right), \left(f_y - \frac{n}{Y}\right)\right] \tag{IV.9a}$$

or equivalently

$$= \tilde{I}_m(f_x, f_y) + \sum_{\substack{m=-\infty \\ (m,\, n) \neq (0,\, 0)}}^{\infty} \sum_{n=-\infty}^{\infty} \tilde{I}_m\left[\left(f_x - \frac{m}{X}\right), \left(f_y - \frac{n}{Y}\right)\right] \tag{IV.9b}$$

where the factor $(XY)^{-1}$ common to all terms has been dropped. Equation (IV.9a) and (IV.9b) can be presented as follows:

$$\tilde{I}_s(f_x, f_y; X, Y) = \tilde{I}_m(f_x, f_y) + \tilde{I}_{ma}(f_x, f_y; X, Y) \tag{IV.10}$$

where the addition of the subscript "a" is intended to indicate aliasing. After substituting (IV. 10) back into (IV. 3) and taking the Fourier transform leads to the reconstructed image spectrum:

$$\tilde{I}_r(f_x, f_y) = \tilde{I}_m(f_x, f_y)H_r(f_x, f_y) + \tilde{I}_{ma}(f_x, f_y; X, Y)H_r(f_x, f_y) \tag{IV.11}$$

The inverse fourier transform of the Equation (IV.11) gives the reconstructed image

signal in the space domain, which is equal to Equation (IV.3):

$$I_r(x,y) = I_{mr}(x,y) + I_{mar}(x,y) \tag{IV.12}$$

$I_{mr}(x,y)$ is the ideal reconstructed image without aliasing and $I_{mar}(x,y)$ is the reconstruction of the higher order terms in which occurs due to sampling [Ref. 38]. The aliasing effect due to the addition of I_{mar}, see Equation (IV.12), can be considered as noise [Ref. 17]. Substitution of (IV.9b) into (IV.10) followed by (IV.11) shows that

$$\tilde{I}_{mr}(f_x, f_y) = \tilde{I}_{mr}(f_x, f_y)\, H_r(f_x, f_y) \tag{IV.13}$$

or from (IV.6)

$$\tilde{I}_{mr}(f_x, f_y) = I(f_x, f_y)\, H_i(f_x, f_y)\, H_r(f_x, f_y) \tag{IV.14}$$

which can be referred as the DC term in (IV.12) since no frequency shifting is involved. The substitution process described above also demonstrates that

$$\tilde{I}_{mar}(f_x, f_y) = \sum_{m=-\infty}^{\infty} \sum_{n=-\infty}^{\infty} \tilde{I}_m(f_x - \tfrac{m}{X}, f_y - \tfrac{n}{Y}) H_i(f_x - \tfrac{m}{X}, f_y - \tfrac{n}{Y}) H_r(f_x, f_y) \tag{IV.15}$$

which includes an infinite number of terms. From this point only the terms with $|n| = |m| = 1$ will be considered significant. Higher order terms, i.e. $n > 1 \quad m > 1$, appear at successively higher multiples of the sampling frequencies (1/X, 1/Y). Since these terms are multiplied in (IV.15) by $H_r(f_x, f_y)$, which is known to be a low pass filter, they are neglected in the subsequent analysis.

B. ANALYSIS AND SIMULATION OF THE ALIASING

The thermal image system, denoted as sample system A, has parameters which are defined in Appendix A. The specifications for this system have been used to generate both the DC reconstruction transfer function $H_i(f_x,f_y)$, $H_r(f_x,f_y)$, see Equation (IV.14), and the first order $|n| = |m| = 1$ transfer function from (IV.15). As previously mentioned the higher orders, i.e $|n| > 1$ $|m| > 1$, are neglected. To demonstrate the aliasing effect the equations described in the previous section will be applied to the parallel scanning TIS, system A, for which only one spatial frequency, f_x, is significant. An adjustment in notation is introduced according to:

$$H_{pre}(f_x) = H_i = H_{opt}(f_x)\,H_{det}(f_x) \tag{IV.16}$$

and

$$H_{post}(f_x) = H_r = H_{elect}(f_x)\,H_{disp}(f_x) \tag{IV.17}$$

which is motivated by noting that previous to sampling the image is affected by both the optics and the averaging effect of the detector window [Ref. 1]. Also after sampling the image signal is affected by both the electronics and the display. It follows from (IV.15) that the first order term, acting as noise, appears as an overlap involving H_r (now known as H_{post}) and a shifted version of H_i (now known as H_{pre}). This motivates the definition:

$$H_{over} = H_{post}(f_x)\,H_{pre}(f_x \pm f_s) \tag{IV.18}$$

where the $\pm$ correspond to n= ± 1, in (IV.15), respectively and f_s= 1/X. This overlap transfer function will be applied to the image spectrum $\tilde{I}_m(f_x)$ shifted by $\pm f_s$. Figure IV.2

shows sketch for the expected frequency dependence of magnitude transfer function for H_{pre}, see Equation (IV.16), H_{post}, see Equation (IV.17), and H_{over}, see Equation (IV.18). Figure IV.3 the corresponding curves for the TIS sample system A.

1. Sample Scene Phasing

The effect of spatially shifting the sampling function relative to a fixed image has been referred to as sample scene phasing. For purposes of evaluating the this effect on the reconstructed image it is necessary to represent the ideal sampling waveform and its spectrum. Figure IV.4 defines the two different cases of interest, i.e ideal sampling waveforms with and without spatial shift.In Case-A, the reference, there is no phase shift due to in the sampling process, but Case-B has a phase shift due to a spatial shift in the sampling process. The exponential Fourier series coefficients, F_n, can be obtained for Case-B by first analyzing Case-A and then using the shift theorem to relate spectrum B to spectrum A. For any periodic function [Ref. 37].

$$F_n = \mathscr{F}_{1D}\{g(x)\} / X \Big|_{f_x = \frac{n}{X}} \qquad \text{(IV.19)}$$

where g(x) is 1 cycle of the periodic waveform centered on x=0 and X is the period of the waveform. For Case-A, see Figure IV.4, g(x)= $\delta(x)$ and X=1/f_s. It follows that

$$F_n^A = f_s \qquad \text{(IV.20)}$$

and therefore after reference to Figure IV.4 and using the shift theorem [Ref. 37]

$$F_n^B = F_n^A \ e^{j2\pi f_x dx} = f_s e^{j2\pi f_x dx}; \qquad \text{(IV.21)}$$

where dx is the spatial shift in the sampling process. Note that dx can be limited to $0 \leq dx \leq 1/f_s$

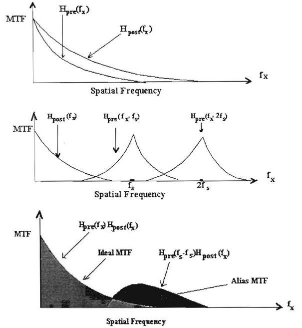

Figure IV.2. Presentation of Aliasing by Using MTF

a. Presampling and Postsampling Transfer Function

b. Presampling Function with Shifted Replica

c. Alias MTF and Ideal MTF

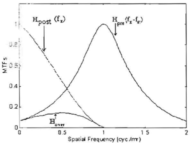

Figure IV.3. $H_{post}(f_x)$, $H_{pre}(f_x\text{-}f_s)$, H_{over} for the Sample System A

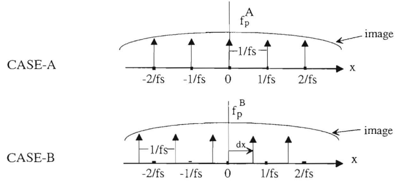

Figure IV.4. Two Different Cases for Sampling Points

Equation (IV.18) can be separated into its real and imaginary parts:

The real part is an even function,

$$\mathrm{Re}\{F_n^B\} = f_s \cos(2\pi n f_s\, dx) \tag{IV.22}$$

The imaginary part is an odd function,

$$\mathrm{Im}\{F_n\} = f_s \sin(2\pi n f_s\, dx) \tag{IV.23}$$

The exponential Fourier series representation for the periodic sampling waveform B is

$$f_p^B(x) = \sum_{n=-\infty}^{\infty} F_n^B\, e^{j2\pi f_s x n} = \sum_{n=-\infty}^{\infty} F_n^B[\cos(n2\pi f_s x) + j\sin(n2\pi f_s x)] \tag{IV.24}$$

By defining F_n in two parts as real and imaginary, Equations (IV.22), (IV.23), Equation

(IV.24) can be written in the following form:

$$f_p^B(x) = \sum_{n=-\infty}^{\infty} [(\mathrm{Re}\{F_n\}\cos(2\pi n f_s x) - \mathrm{Im}\{F_n\}\sin(2\pi n f_s x)) + j(\mathrm{Im}\{F_n\}\cos(2\pi n f_s x) + \mathrm{Re}\{F_n\}\sin(2\pi n f_s x))] \quad \text{(IV.25)}$$

By substituting the real and imaginary F_n from Equation (IV.22) and (IV.23) to (IV.25) leads to a simpler expression

$$f_p^B(x) = f_s + 2\sum_{n=1}^{\infty} [\cos(2\pi n f_s dx)\cos(2\pi n f_s x) - \sin(2\pi n f_s dx)\sin(2\pi n f_s x)] \quad \text{(IV.26)}$$

where a factor of 2 accounts for terms having a negative index in (IV.25). When n is equal to zero, (IV.25) gives the DC component of the sampling function:

$$f_{p_0}^B(x) = f_s \quad \text{(IV.27)}$$

When n is equal to one, Equation (IV.26) gives the term, which is used in the subsequent calculations to estimate the aliasing effect:

$$f_{p_1}^B(x) = 2f_s[\cos(2\pi f_s dx)\cos(2\pi f_s x) - \sin(2\pi f_s dx)\sin(2\pi f_s x)] \quad \text{(IV.28)}$$

which can be simplified in the following way:

$$f_{p_1}^B(x) = 2f_s \sin[2\pi f_s(x + dx) + \tfrac{\pi}{2}] \quad \text{(IV.29)}$$

2. Calculation Of The Aliasing

The input image signal, a periodic square wave of period f_x^{-1}, is given in Equation (IV.27) [Ref.8]:

$$I(f,x) = \frac{1}{2} + \sum_{n=1,3,5\ldots}^{\infty} \frac{1}{n} \sin(2\pi n f_x x) \qquad \text{(IV.30)}$$

which provides for MRTD analysis, a convenient mathematical approximation to a four-bar pattern. Multiplication of the first order term from the sampling function which is Equation (IV.29), with the input image signal, Equation (IV.30), gives the first order spectral replica of the image signal, which is centered due to sampling. Equation (IV.27) shows that when n is equal to zero, the DC component is equal to f_s. Because the DC spectral replica is the ideal reference which is not included in the following equation, this first factor is non-essential, and we can write

$$I'(x,f) = \sin(2\pi f_s(x+dx)+\tfrac{\pi}{2}) + 2\sum_{n=1}^{\infty}\tfrac{1}{n}[\cos(2\pi(f_s-nf)\,x+2\pi f_s dx+\tfrac{\pi}{2}) - \cos(2\pi(f_s+nf)x + 2\pi f_s dx + \tfrac{\pi}{2})] \qquad \text{(IV.31)}$$

Equation (IV.31) can be simplified by defining the three terms:

$$\text{Term1}=\sin(2\pi f_s(x+dx)+\tfrac{\pi}{2}) \qquad \text{(IV.32a)}$$

$$\text{Term2}=2\sum_{n=1,3,5\ldots}^{\infty}\tfrac{1}{n}[\cos(2\pi(f_s-nf)\,x+2\pi f_s dx+\tfrac{\pi}{2}) \qquad \text{(IV.32b)}$$

$$\text{Term3}=2\sum_{n=1,3,5\ldots}^{\infty}\tfrac{1}{n}[\cos(2\pi(f_s+nf)x + 2\pi f_s dx + \tfrac{\pi}{2}) \qquad \text{(IV.32c)}$$

It can then be is rewritten by using these three terms, as

$$I'(x,f) = \text{Term1} + \text{Term2} - \text{Term3} \tag{IV.32d}$$

Since the image is filtered by H_{pre} prior to sampling the alias OTF, shown in Figure IV.2, needs to operate on the shifted image. Figure IV.5 defines the effects of a transfer function, H, on an input sinusoid.

$$OTF' = |H_{post}(f_x)|\,|H_{pre}(f_x - f_s)|\,e^{j[\angle PTF_{pre}(f_x - f_s) + \angle PTF_{post}(f_x)]} \tag{IV.33}$$

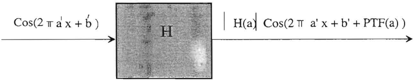

Figure IV.5. The H-Rule (a' and b' are arbitrary constants)

Equation (IV.32.a-d) and (IV.33) gives the aliasing term, which can be written by using Term1, Term2, and Term3.

$$A = OTF'(\text{Term1}) + OTF'(\text{Term2}) + OTF'(\text{Term3}) \tag{IV.34}$$

when

$$OTF'(\text{Term1}) = \tfrac{1}{2}|H_2(f_s)|\,|H_1(0)|\,\sin[2\pi f_s(x + dx) + \tfrac{\pi}{2} + PTF_2(f_s) + PTF_1(0)] \tag{IV.35a}$$

$$OTF'(\text{Term2}) = \sum_{n=1}^{\infty} \tfrac{1}{n}|H_2(f_s - nf)|\,|H_1(-nf)|\cos(2\pi(f_s - nf)x + 2\pi f_s dx + \tfrac{\pi}{2} + PTF_2(f_s - nf) + PTF_1(-nf)) \tag{IV.35b}$$

and

$$OTF'(\text{Term3}) = -\sum_{n=1}^{\infty} \frac{1}{n} |H_2(f_s + nf)||H_1(nf)| \cos(2\pi(f_s + nf)x + 2\pi f_s dx + \frac{\pi}{2} + PTF_2(f_s + nf) + PTF_1(nf)) \quad \text{(IV.35c)}$$

where for compactness subscript 2 denotes pre and subscript 1 denotes post. It is important to note that consistent with the symmetry conditions of transfer function [Ref.37] the magnitude is an even function about DC and the phase is an odd function about DC. Equation (IV.34) shows the first order aliasing term. Higher order aliasing terms are not significant as it can be seen from Figure IV.5. In Equations (IV.35.a-c), H_1 and H_2 are used for the terms which are shown in the following equations. PTF_1 is used for detector and PTF_2 is used for electronics.

$$H_1 = H_{post} = H_{elect} H_{disp} \quad \text{(IV.36a)}$$

and

$$H_2 = H_{pre} = H_{opt} H_{det} \quad \text{(IV.36b)}$$

3. Simulation of the Aliasing

The sample system, which is given in Appendix A, is used to simulate the aliasing. In this simulation dx is 0.1 mrad, and spatial frequency is 0.15 cyc/mrad. Figure IV.5 shows the square wave image signal and expected image output signal with phase shift, because of the phase transfer function of the system. Figure IV.6 presents the expected image output signal and aliasing, which was defined by Equation (IV.24). Figure IV.7 shows the square wave image signal and output image with aliasing. Figure IV.8 is the presentation of the square wave input image signal, expected image output, and output image with aliasing. These figures show that aliasing can be considered as an additional noise and causes distortion on the expected output image signal.

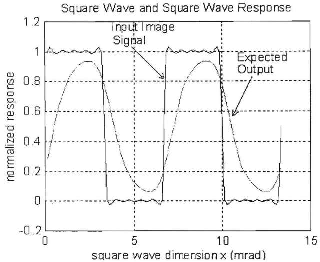

Figure IV.5. Square Wave Image Signal and Expected Image Output Signal

(After Ref. [8])

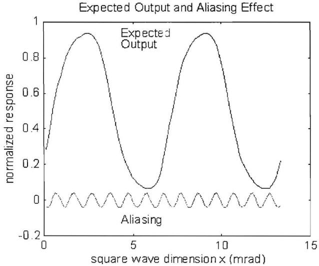

Figure IV.6. Expected Image Output Signal and Aliasing

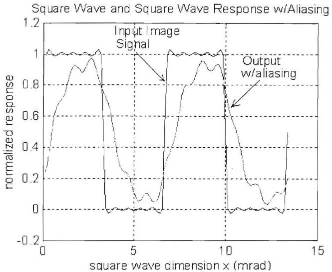

Figure IV.7. Square Wave Image Signal and Image Output with Aliasing

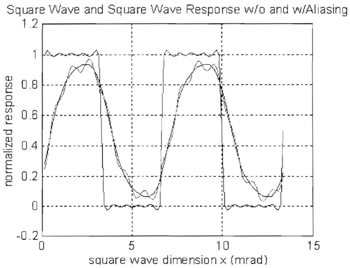

Figure IV.8. Square Wave Image Signal, Expected Image Output

C. REDUCING THE ALIASING EFFECT

There are different methods to reduce the amount of the aliasing (Ref. [18]):

1. Increasing the fill factor to 100%
2. Increasing the sampling rate by decreasing the FOV
3. Increasing the number of detectors
4. Microscanning

The first three of these methods have some fabrication problems and they are not preferred. That is why microscanning will be presented as a method to reduce the aliasing for staring systems (Ref. [18]).

1. Microscanning Process

In this technique, FOV of the detector is shifted around by increments relative to the scene. This shifting distance is related to the spacing between the detectors, and amount of the shifting depends on the desired microscanning level. Figure IV.9 shows the shifting of the FOV.

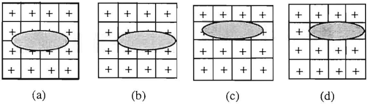

Figure IV.9. Microscanning Process

Equation (IV.2) will be used to represent the sampled image, and it is rewritten in the following equation:

$$I_s(x,y;X,Y) = I_m(x,y)P_s\left[\left(\frac{x}{X}\right),\left(\frac{y}{Y}\right)\right] \tag{IV.37}$$

The ideal sampling function can be defined in the following way:

$$P_s\left[\left(\frac{x}{X}\right),\left(\frac{y}{Y}\right)\right] = \frac{1}{XY}comb\left[\left(\frac{x}{X}\right),\left(\frac{y}{Y}\right)\right] \tag{IV.38}$$

where the comb function is used to represent an infinite array of uniformly spaced impulses [Ref. 38]. By using Equation (IV.37) and (IV.38), the sampled image signal can be rewritten as follows:

$$I_s(x,y;X,Y) = \left[\frac{1}{d_x d_y}b\left(\frac{x}{d_x},\frac{y}{d_y}\right) * I(x,y) * h_i(x,y)\right]\times \tag{IV.39}$$

$$\left(\frac{1}{XY}\right)comb\left[\left(\frac{x}{X}\right),\left(\frac{y}{Y}\right)\right]$$

where Equation IV.1 has been used to relate the image to the scene. In this equation $b\left(\frac{x}{d_x},\frac{y}{d_y}\right)$ is the shape of the each pixel and d_x, d_y are the widths of the pixels in the relative directions. If four microscan steps, shown in Figure (IV.8), are applied to this image signal, the linear superposition of "snapshots" taken during 1 cycle of the microscan process can be represented in the following way:

$$\begin{aligned} I_s(x,y;X,Y) = \frac{1}{4}&\left[\frac{1}{d_x d_y}b\left(\frac{x}{d_x},\frac{y}{d_y}\right) * I(x,y) * h_i(x,y)\right]\times \\ &\frac{1}{XY}\{comb(\tfrac{x}{X},\tfrac{y}{Y}) + comb(\tfrac{x}{X}-\tfrac{1}{2},\tfrac{y}{Y}) + \\ &comb(\tfrac{x}{X},\tfrac{y}{Y}-\tfrac{1}{2}) + comb(\tfrac{x}{X}-\tfrac{1}{2},\tfrac{y}{Y}-\tfrac{1}{2})\} \end{aligned} \tag{IV.40}$$

Equation (IV.40) shows that integration time is increased by a factor of 4, because the image signal is integrated four times for one sampled image signal. The Fourier transform

equation is written as follows:

$$I_s(f_x,f_y;X,Y) = \tfrac{1}{4}\tilde{b}(f_x d_x, f_y d_y)\tilde{I}(f_x,f_y)H_i(f_x,f_y) \times; \quad \text{(IV.41)}$$
$$comb(f_x X, f_y Y)\{1 + e^{-i\pi f_x X} + e^{-i\pi f_y Y} + e^{-i\pi(f_x X + f_y Y)}\}$$

By using Equation (IV.5), it can be defined in the following form:

$$I_s(f_x,f_y;X,Y) = \tfrac{1}{4}\left[\tilde{b}(f_x d_x, f_y d_y)\tilde{I}(f_x,f_y)H_i(f_x,f_y)\right] \times; \quad \text{(IV.42)}$$
$$\sum_{m=-\infty}^{\infty}\sum_{n=-\infty}^{\infty} \delta(f_x X - n, f_y Y - m)\{1 + e^{-i\pi n} + e^{-i\pi m} + e^{-i\pi(n+m)}\}$$

which follows after noting that the localized contribution of the impulses permits the sum of complex exponentials in (IV.41) evaluated at $f_x = \frac{n}{X}$ and $f_y = \frac{m}{Y}$. The final step is Equation (IV.42), which reduces to zero, if both m and n are not even. It removes the odd harmonics and decreases the amount of the overlap. Figure (IV.9) shows this process.

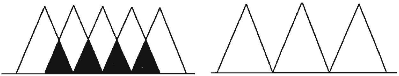

a. Harmonics overlap each other   b. Odd Harmonics are removed

Figure IV.10. Removing Odd Harmonics by Microscanning

V. LABORATORY MEASUREMENTS

To compare the FLIR92 TISs Performance Model to the measured data for second generation TISs, two laboratory measurements were done. An Amber Engineering- AE4128 IR Imaging System and a Mitsubishi Electronics IR-M500 Imager were used for these experiments. These two systems' parameters are given in Appendix A. Comparison of these measurements to FLIR92 is shown in Chapter VI.

A. LABORATORY SETUP

Figure V.1 shows the laboratory setup used for both of the measurements. The oscilloscope, which is shown in this figure, was used only for the Mitsubishi IR-M500 experiment as an Automatic Target Recognition (ATR) unit.

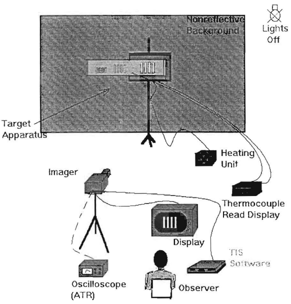

Figure V.1. Laboratory Setup

Aluminum was used for the target plates, painted in a non-reflective flat black to have uniform emissivity. A variable heater was used to heat the back plate. Front plate was placed 10 cm. in front of the back plate to keep it at ambient temperature. Four bar patterns which were cut through the front plate had standard size with , length equal to seven times the width, to give different spatial frequencies related to the distance from the target to the imager. The thermocouple read-out displays had one digit decimal precision; to have more precise reading, these displays were used in Fahrenheit mode, provided $\pm 0.0556°C$ tolerance. This tolerance limited the precision of the measurements.

The target apparatus was placed in front of a non-reflective background to minimize the reflective radiance from the environment.

1. Amber Engineering AE4128 IR Imaging System

The Amber system is a 128×128 Indium Antimonide staring array, which operates in the 3-5 μm. wavelength band. Its display provides gray-scale shading or pseudocolor. The camera assembly has a cyrogenic dewer, which is filled with liquid nitrogen to keep the detector temperature around 77°K. Its capacity is 400 ml. To provide this temperature level and to prevent the condensation on the detector this dewer needs to be evacuated to less than 10^{-4} torr. The operator can control contrast, global gain, global offset, integration time, and frame rate to adjust the camera [Ref. 24]. In this experiment global gain was set to one, global offset was adjusted to zero, frame rate was 109 Hz, and integration time was 62. The two point calibration method [Ref. 24] was used to calibrate the system. Figure V.2 is a picture of the Amber camera.

2. Mitsubishi Electronics IR-M500 Thermal Imager

This system does not need any external cooling process. The *Mitsubishi* camera has a cyrogenic stirling cycle cooler to keep the detector temperature around 80°K. This is a 512×512 PtSi staring array, which operates in the 3-5 μm. wavelength band operator

has a small wired remote controller and can not control the most of the features. This system' s picture is shown in Figure V.3.

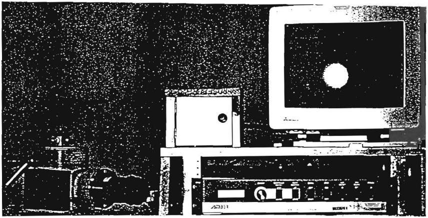

Figure V.2. Amber AE4128 IR Imaging System

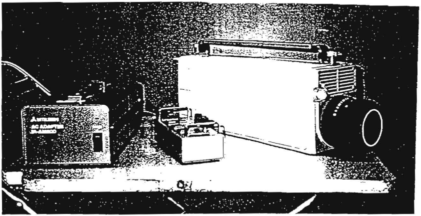

Figure V.3. Mitsubishi IR-M500 Thermal Imager

B. PROCEDURE

As a first step the input aperture lens of the TIS and the target bar pattern were adjusted to the same height and then aligned perpendicular to each other. As a second step each TIS was calibrated. The laboratory was darkened during the measurements. To familiarize the observers with four bar pattern' s position and view on display the background plate was heated up and observer was allowed to adjust the camera and his position to have optimum view. During the measurements observers knew where to look on the display for the four bar pattern. Measurements were done in two stages for each system with multiple observers. In the first stage the background plate was heated up until the observer decided that four bar pattern was 100% resolvable, then the temperature difference between the thermocouple readings were recorded as the MRTD. In the second stage, the backplate was cooled down, via air cooling, until the observer could not resolve 100% of the four bar pattern and again the temperature difference was recorded as an MRTD. These steps were repeated for different spatial frequencies. An entire set of measurements were taken by one observer , then same process was done by another observer. This process was repeated for both horizontal and vertical directions in order to characterize the MRTD values in these directions and to calculate the $MRTD_{2D}$.

C. EXPERIMENTAL MRTD MEASUREMENTS

MRTD measurements showed that $MRTD_v$ has a higher value, or equivalently a lower performance, than $MRTD_h$ for both of the systems. Figure V.4. shows the $MRTD_h$, $MRTD_v$, and $MRTD_{2d}$ curves for Amber AE4128 IR Imaging System. $MRTD_{2d}$ was calculated from $MRTD_v$ and $MRTD_h$ using Equation (III.13). Figure V.5. is the logarithmic presentation of the same values. Figure V.6 shows the $MRTD_h$, $MRTD_v$, and $MRTD_{2d}$ values for Mitsubishi IR-M500 Thermal Imager. Figure V.7 presents the same values in logarithmic scale [Ref. 27].

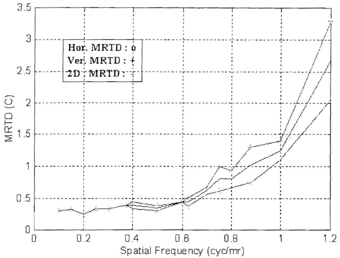

Figure V.4.MRTD Measurements for Amber AE4128 IR Imaging System

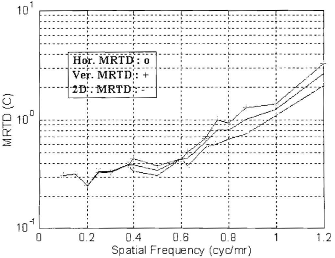

Figure V.5. Logarithmic Presentation of the MRTD Measurements for Amber AE4128 IR Imaging System

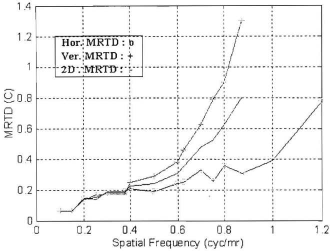

Figure V.6. MRTD Measurements for Mitsubishi IR-M500 Thermal Imager

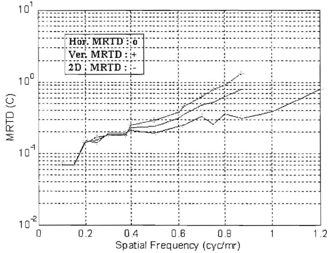

Figure V.7. Logarithmic Presentation of the MRTD Measurements for Mitsubishi IR-M500 Thermal Imager

D. OBJECTIVE MEASUREMENTS

These experiments were done with the Mitsubishi System and instead of a human observer an oscilloscope was used to model an ATR. Three different sets of measurement were taken.

1. Constant SNR

For objective MRTD measurements the acceptable SNR was set to 6.0 which gives reasonable target resolution on the measurement device, an oscilloscope. Using the oscilloscope ΔV_{signal} and ΔV_{noise} were measured and their ratio used as the SNR. When SNR reached 6.0, the temperature difference between the front and back plate was recorded for four bar patterns of different spatial frequencies. Figure V.8 shows that MRTD measured with Tektronix 468 Digital Storage Oscilloscope. This value for MRTD is much higher than the MRTD measured by the human observer. The MRTD value can change from observer to observer, but the objective MRTD is more reproducible.

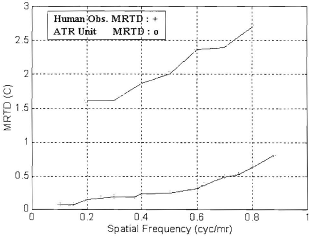

Figure V.8. Comparison of MRTD Measured by ATR to MRTD Measured by Human Observer for Mitsubishi System

Figure V.9. presents the picture, which shows the four bar pattern view on the display and ATR unit display, when spatial frequency is 0.8 cyc/mr, temperature difference between the plates is 2.69 °C and SNR is 6.0.

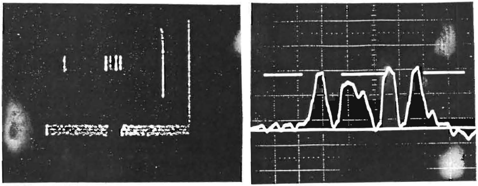

a. Target View on the Display b. ATR Unit Display

Figure V.9. The View of the Target on the Monitor and ATR Unit Display

From the picture of the display, Figure V.9b, noise level is measured as 0.4 unit and signal level is measured as 2.4 unit. The ratio of the signal level to the noise level gives 6.0 as accepted. The defined SNR threshold of 6.0 is selected arbitrarily.

2. Constant Temperature

In a second set of measurements the temperature difference between the plates was kept constant, 1.94 °C, and SNR was measured by using the ATR unit for different spatial frequencies. Figure V.10 presents the results of this measurement. Figure V.8 shows that a 1.92 °C temperature difference between the plates is needed to have SNR equal to 6.0, when the spatial frequency is 0.4 cyc/mr. If this result is compared to the

Figure V.10, it is seen, as expected, that SNR starts to go down for values higher than 0.4 cyc/mr.

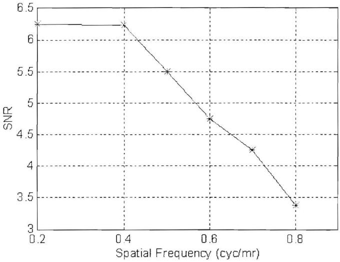

Figure V.10 SNR for Different Spatial Frequencies at Constant Temperature, 1.92 °C, by Using ATR

3. Constant Spatial Frequency

In a third set of measurements the spatial frequency was chosen constant at 0.5 cyc./mr. and a temperature difference between the plates was recorded for the various SNR levels, which were measured by ATR, from 1.0 to 8.0. The results of the measurement are presented in Figure V.11 As expected SNR level increases temperature difference between the plates increases.

These three objective measurements demonstrated the interesting relationships between the SNR, temperature difference between the plates, and spatial frequency,

keeping one of them constant each time. At the same time the ATR unit MRTD was compared to the subjective MRTD.

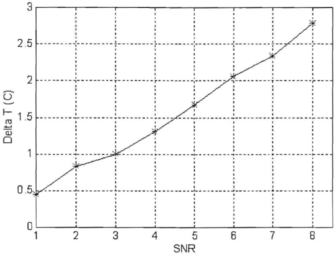

Figure V.11. SNR vs. Delta T (°C) at 0.5 cyc./mr Spatial Frequency

This comparison (Figure V.8) shows the oscilloscope-measured MRTD to exceed the "subjective" value by a factor of approximately 5. This factor is strongly influenced by the choice of "threshold" SNR. From Figure V.9.b we see that the oscilloscope clearly exceeds the noise: this must be considered well above threshold. Figure V.9.a is also seen to be clearly resolved. Thus the selection 6.0 clearly exceeds the threshold value of SNR needed for subjective MRTD evaluation, and the objective "MRTD" curve is artificially elevated. A lower threshold SNR selection would bring the "subjective" and "objective" curves of MRTD into closer agreement. However, it was discovered that if a significantly lower SNR (i.e., SNR=2) was employed in the oscilloscope measurement then the pattern appearing on the oscilloscope display was not always identifiable as a four bar pattern.

VI. COMPARISON OF FLIR92 MRTD TO MEASURED MRTD AND CONCLUSION

A. COMPARISON OF FLIR92 MRTD TO MEASURED MRTD

MRTD measurements, which made with the Amber Engineering AE4128 IR Imaging System and Mitsubishi Electronics IR-M500 Thermal Imager, were presented in Chapter V. This chapter compares the measured MRTD values to the predicted FLIR92 MRTD values. Short output listings of the FLIR92 code for both of the systems are presented in Appendix D.

1. Amber Engineering AE4128 IR Imaging System

Predicted FLIR92 $MRTD_h$, $MRTD_v$, and $MRTD_{2d}$ for the Amber system can be seen in Figure VI.1. Figure VI.2 compares the FLIR92 and measured $MRTD_{2d}$. Figure VI.3 is the logarithmic presentation of the same comparison. These figures show that predicted FLIR92 MRTD is more optimistic than the measured MRTD by a factor of about one hundred. Figure VI.1 shows predicted MRTD of the functional form expected, and similar shape to the measurements shown in Figure VI.2. However discrepancy in magnitude of about a hundred is seen between prediction and measurement. Reasons for this may be sought in the input to prediction and in the experience level of the operators making the measurements. The FLIR92 MRTD value assumes "experienced operators", which makes it unrealistic for our measurements. Additionally the Amber system is an Indium Antimonide Focal Plane Array sensor, which necessitates input of spectral detectivity for InSb.

2. Mitsubishi Electronics IR-M500 Thermal Imager

Predicted FLIR92 $MRTD_h$, $MRTD_v$, and $MRTD_{2d}$ for Mitsubishi system are presented in Figure VI.4. Figure VI.5 is the comparison of the FLIR92 $MRTD_{2d}$ to the measured $MRTD_{2d}$. Figure VI.6 shows this comparison in logarithmic scale. Predicted FLIR92 MRTD is better than measured MRTD, but these values are closer to each other than Amber system's values. The corresponding comparison for the Mitsubishi system (Figure VI.5) shows much closer agreement, with again, the modeled MRTD being more optimistic (lower) than the measured. The discrepancy is now in the range of 50% of predicted, which might be accounted for by the experience factor in the operators.

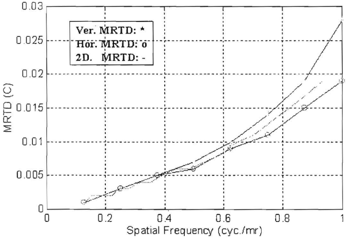

Figure VI.1. FLIR92 MRTD Values for Amber System

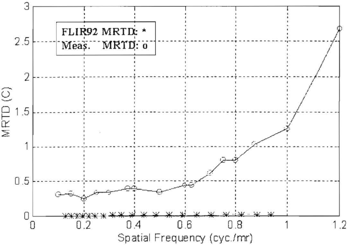

Figure VI.2. Comparison of the FLIR92 MRTD to the Measured MRTD for Amber System

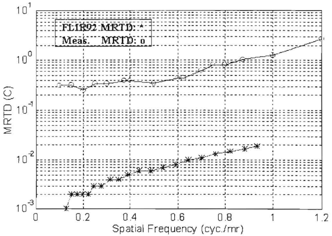

Figure VI.3. Logarithmic Comparison of the FLIR92 MRTD to the Measured MRTD for Amber System

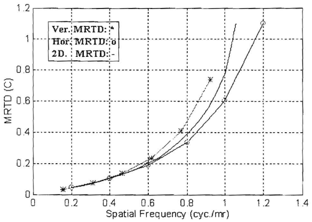

Figure. VI.4. FLIR92 MRTD Values for Mitsubishi System

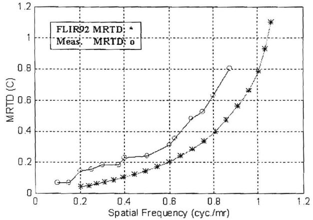

Figure VI.5. Comparison of the FLIR92 MRTD to the Measured MRTD for Mitsubishi System

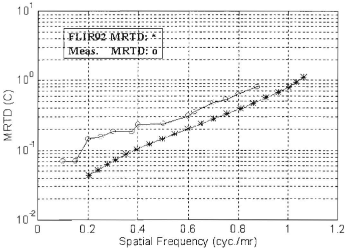

Figure VI.6. Logarithmic Comparison of the FLIR92 MRTD to the Measured MRTD for Mitsubishi System

B. LIMITATIONS OF THE FLIR92 AND CONCLUSION

1. FLIR92 TIS Performance Model's 3D noise concept was covered in Chapter III. Only NVEOD has the necessary technology to measure these 3D noise components. For this reason default noise values were used in the applications.

2. FLIR92 does not cover the aliasing effect. For this reason it does not make any MRTD prediction for spatial frequencies higher than the Nyquist Frequency. The aliasing effect was mentioned in Chapter IV, FLIR92 needs to include this effect to make MRTD predictions for spatial frequencies higher than the Nyquist Frequency.

3. FLIR92 does not predict the MRTD correctly at low spatial frequencies, its value is optimistic [Ref. 2 .p. 397].

4. The FLIR92 validation data base includes only PtSi and HgCdTe sensors for staring systems. For this reason the detectivity curve for Amber Indium Antimonide staring array was identified by using spectral detectivity data at three wavelength points.

The Mitsubishi PtSi staring array system did not need to be defined by spectral detectivity data. Comparisons of the FLIR92 MRTD values to the measured MRTD values show that there is big difference between measured and predicted MRTD for the Amber System, whereas the values for the Mitsubishi System are close together. If Indium Antimonide is added to the FLIR92 validation data base, the MRTD predictions for this system may be closer to the measured values.

5. Explanations and equations, which are given in Ref.(9) and (10), are not adequate to describe the FLIR92 TIS Performance Model exactly. Source code for this model is needed to make this system concept clearer and to prepare a background for future studies.

6. FLIR92 does not plot the predicted output values. A plot program is needed to plot the outputs.

APPENDIX A. THERMAL IMAGING SYSTEM PARAMETERS

A. SAMPLE FIRST GENERATION SYSTEM

In Chapter II to present Ratches Model, Lloyd Model, and FLIR92 Model this sample system was chosen in similarity with the one employed by Lloyd [Ref. 1] and used in Reference 3. The parameters of this system are as follows:

Lens focal length (d) 50000μm
Diameter of lens (D) 20000μm
F/ number 2.5
Detector array individual element size (square) 0.005cm
α 1mrad
β 1mrad
Detectors cold shielding .... not background limited
Characteristic wavelength of the detectors 11.5μm
Spectral bandpass of the detectors .... 8μm – 11.5μm
Specific detectivity .... 2×10^{10} cm $Hz^{0.5}$/watt
Frame rate .... 30 Hz
Scan rate format .... 60 fields/sec
Number of detectors in parallel 150
Number of scan lines 300
Interlace .... 2 to 1
Horizontal scan efficiency 0.8
Vertical scan efficiency 0.8
Overall scan efficiency 0.64
Overscan ratio 1
Distance between horizontal scan lines 1mrad
HFOV 400mrad
VFOV 300mrad
Detector dwell time .... 2.67×10^{-5} sec

Horizontal scanning velocity 37453.2mrad/sec
3-dB freq. electronic roll-off...18716.6 Hz
Noise equivalent reference bandwidth...29.4KHz
SNR_{th} for detection of one bar.. 4.5
Background temperature...300°K
Monochromatic wavelength of the target..10μm
Optical efficiency of the viewer... 0.8

B. SECOND GENERATION SYSTEMS

The Amber Engineering AE4128 IR Imaging System and Mitsubishi Electronics IR-M500 Thermal Imager were used for laboratory measurements and their results were compared to predicted FLIR92 values. The parameters of these systems are as follows:

1. Amber Engineering AE4128 IR Imaging System

BLIP Performance..YES
Spectral cut-on...3.0 μm
Spectral cut-off...5.0 μm
F/ number...3.0
Focal length..10.0 cm
Optical transmittance...0.95
Frame rate...109 Hz
Detector active horizontal dimension..40 μm
Detector active vertical dimension..40 μm
D^*..5.97×10^{11} cm $Hz^{0.5}$/watt
Integration time..8887.615 μ sec
Number of horizontal detectors..128
Number of vertical detectors...128
Detector cell horizontal dimension..50 μm

Detector cell vertical dimension..50 μm

Number of active CRT lines..480

Display brightness..10.0 mLamberts

3D noise level...MOD

2. Mitsubishi Electronics IR-M500 Thermal Imager

BLIP performance...YES

Spectral cut-on...3.0 μm

Spectral cut-off..5.0 μm

F/ number...1.4

Focal length...5.0 cm

Optical transmittance..0.95

Frame rate...60 Hz

Detector active horizontal dimension...16.24 μm

Detector active vertical dimension...12.49 μm

D^*...5.0×10^{10}cm $Hz^{0.5}$/watt

Integration time..16145.833

Number of horizontal detectors...512

Number of vertical detectors...512

Detector cell horizontal dimension...26 μm

Detector cell vertical dimension..20 μm

Number of active CRT lines..480

PtSi emission coefficient...0.16 1/eV

Schottky barrier height...22 eV

Display brightness..10.0 mLamberts

3D noise level...MOD

APPENDIX B. FLIR92 MTF EQUATIONS AND D OPERATOR

FLIR92 TIS Performance Model was covered in Chapter III. This appendix gives all MTF equations used in FLIR92 (Ref. [9]) and a different approach to the usage of D operators.

A. MTF EQUATIONS

1. Prefilter MTFs

a. Optics MTFs

(1) Diffraction-limited MTF

$$H_{odl} = \frac{2}{\pi}\left[a\cos\left(\frac{\lambda f}{D_o}\right) - \left(\frac{\lambda f}{D_o}\right)\left(1-\left(\frac{\lambda f}{D_o}\right)^2\right)^{0.5}\right] \quad (A.1)$$

(2) Geometric Blur MTF

$$H_{ogb}(f) = e^{\left(-2\pi^2\sigma^2 f^2\right)} \quad (A.2)$$

b. Detector Spatial MTF

$$H_{ds}(f) = \frac{\sin(\pi\delta_z f)}{\pi\delta_z f} \quad (A.3)$$

c. Focal Plane Array Integration Time

$$H_{di}(f) = \frac{\sin(\pi f_t v_x t_i)}{\pi f_t v_x t_i} \quad (A.4)$$

d. Sample-scene Phase MTF

$$H_{ssp}(f) = \cos\left(\frac{f}{f_n}\theta_z\right) \tag{A.5}$$

e. Image Motion MTFs

(1) Linear Image Motion MTF

$$H_{ml}(f) = \frac{\sin(\pi v_r t_i f)}{\pi v_r t_i f} \tag{A.6}$$

(2) Random Image Motion MTF

$$H_{mr}(f) = e^{\left(-2\pi^2 \sigma^2 f^2\right)} \tag{A.7}$$

(3) Sinusoidal Image Motion MTF

$$H_{ms}(f) = J_o(2\pi A f) \tag{A.8}$$

2. Temporal Postfilter MTFs

a. Detector Temporal MTF

$$H_{dt}(f_t) = \left(1 + \left(\frac{f_t}{f_{3dB}}\right)^2\right)^{0.5} \tag{A.9}$$

b. Electronics Low Frequency Response

$$H_{ehp}(f_t) = \frac{\left(\frac{f_t}{f_{ehp}}\right)^n}{\left(1+\left(\frac{f_t}{f_{ehp}}\right)^{2n}\right)^{0.5}} \tag{A.10}$$

c. Electronics High Frequency Response

$$H_{elp}(f_t) = \left(1 + \left(\frac{f_t}{f_{elp}}\right)^{2n}\right)^{-0.5} \tag{A.11}$$

d. Boosting MTF

$$H_{eb}(f_t) = 1 + \frac{B_a - 1}{2}\left(1 - \cos\left(\frac{\pi f_t}{f_b}\right)\right) \tag{A.12}$$

3. Spatial Postfilter MTFs

a. Electro-optical Multiplexor MTF

$$H_{eom}(f) = \frac{\sin(\pi f \delta_{led})}{\pi f \delta_{led}} \tag{A.13}$$

b. Digital Filter MTF

$$H_{dlg}(f) = \sum_{i=0}^{(N-1)/2} a_i \cos\left(\frac{2\pi i f}{f_{co}}\right) \quad \text{if N is odd} \tag{A.14}$$

$$H_{dlg}(f) = \sum_{i=1}^{N/2} a_i \cos\left(\frac{2\pi (i-0.5) f}{f_{co}}\right) \quad \text{if N is even} \tag{A.15}$$

c. Display MTF

(1) CRT Display MTF

$$\sigma = \left(\frac{-\log(0.025)}{2\pi^2\left(\frac{N_r}{\beta}\right)^2}\right)^{0.5} \tag{A.16}$$

$$H_{crt}(f) = e^{(-2\pi^2 \sigma^2 f^2)} \tag{A.17}$$

d. CCD Charge Transfer Efficiency MTF

$$H_{ccd}(f) = e^{\left(-N_{ccd}(1-\varepsilon)\left(1-\cos\left(\frac{2\pi f}{f_n}\right)\right)\right)} \tag{A.18}$$

e. Display Sample and Hold MTF

$$H_{dsh}(f) = \frac{\sin(\pi \delta_s f)}{\pi \delta_s f} \tag{A.19}$$

f. Eye MTF

(1) Non-limiting Eye MTF

$$H_{eye}(f) = 1.0 \tag{A.20}$$

(2) Limiting Eye MTF

$$H_{eye}(f) = e^{\left(\frac{-\Gamma f}{2M_g}\right)} \tag{A.21}$$

B. DIRECTIONAL AVERAGING OPERATOR (D OPERATOR)

Reference 12 brings another approach to the usage of D operators. In this approach by applying D_t, D_v, or D_h operations to the noise components and by using subtraction between the noise data sets, we extract a desired noise component. As an example, if we want to find N_{th}, the following steps must be applied, which are shown in Figure III.3:

a. Apply D_t and D_v to the composite data set:

(1) D_t process gives data set-1: N_{vh}, N_v, N_h, and s

(2) D_v process gives data set-2: N_{th}, N_h, N_t, and s

b. Apply D_v to the data set-1 to obtain the data set-3: N_h and s

c. Subtract the data set-3 from the data set-2 to have data set-4: N_{th} and s

d. Apply D_t to the data set-3 to obtain the s-component

e. Subtract s-component (step. d) from data set-4. This gives the final data set which has only N_{th} .

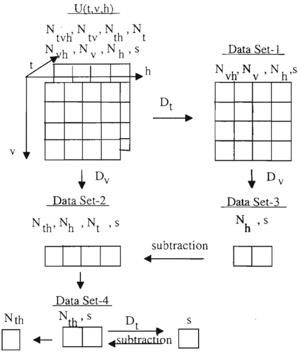

Figure B.1. Application of D Operator

APPENDIX C. LABORATORY MEASUREMENTS

This appendix presents the measured data, which is mentioned in Chapter V and shows plots of MRTD measured during the heating and cooling cycles in horizontal and vertical directions for the Amber and Mitsubishi systems.

Table C.1. Amber System Measured $MRTD_h$

Spatial Freq. (cyc./mr)	MRTD-Heating (°C)	MRTD-Cooling (°C)	Average MRTD (°C)
0.1	0.33	0.28	0.31
0.15	0.33	0.31	0.32
0.2	0.33	0.17	0.25
0.25	0.28	0.39	0.34
0.3	0.36	0.31	0.34
0.375	0.33	0.44	0.39
0.4	0.39	0.28	0.34
0.50	0.33	0.28	0.31
0.60	0.44	0.44	0.44
0.625	0.42	0.33	0.38
0.70	0.56	0.56	0.56
0.75	0.61	0.61	0.61
0.80	0.58	0.75	0.67
0.875	0.67	0.83	0.75
1.0	0.78	1.6	1.11
1.2	1.5	2.6	2.05

Table C.2. Amber System Measured $MRTD_v$

Spatial Freq. (cyc./mr)	MRTD-Heating (°C)	MRTD-Cooling (°C)	Average MRTD (°C)
0.10	0.33	0.28	0.31
0.15	0.33	0.31	0.32
0.20	0.33	0.17	0.25
0.25	0.28	0.39	0.33
0.30	0.36	0.31	0.33
0.375	0.39	0.39	0.39
0.40	0.44	0.44	0.44
0.50	0.19	0.56	0.38
0.60	0.25	0.64	0.44
0.625	0.42	0.61	0.51
0.70	0.56	0.81	0.68
0.75	1.1	0.89	1.0
0.80	1.1	0.83	0.94
0.875	1.6	1.0	1.3
1.0	1.6	1.1	1.4
1.2	3.3	3.3	3.3

Table C.3. Mitsubishi System Measured $MRTD_b$

Spatial Freq. (cyc./mr)	MRTD-Heating (°C)	MRTD-Cooling (°C)	Average MRTD (°C)
0.10	0.08	0.06	0.07
0.15	0.08	0.06	0.07
0.20	0.12	0.18	0.15
0.25	0.15	0.13	0.14
0.30	0.28	0.11	0.19
0.375	0.26	0.13	0.19
0.40	0.28	0.14	0.21
0.50	0.26	0.13	0.19
0.60	0.28	0.19	0.24
0.625	0.31	0.19	0.25
0.70	0.36	0.31	0.33
0.75	0.28	0.25	0.26
0.80	0.36	0.36	0.36
0.875	0.31	0.31	0.31
1.0	0.44	0.33	0.39
1.2	0.78	0.78	0.78

Table C.4. Mitsubishi System Measured $MRTD_v$

Spatial Freq. (cyc./mr)	MRTD-Heating (°C)	MRTD-Cooling (°C)	Average MRTD (°C)
0.10	0.08	0.06	0.07
0.15	0.08	0.06	0.07
0.20	0.17	0.11	0.14
0.25	0.22	0.11	0.17
0.30	0.25	0.11	0.18
0.375	0.22	0.14	0.18
0.40	0.39	0.11	0.25
0.50	0.39	0.19	0.29
0.60	0.44	0.31	0.38
0.625	0.44	0.47	0.46
0.70	0.81	0.44	0.63
0.75	0.83	0.75	0.79
0.80	1.1	0.70	0.90
0.875	1.3	0.69	1.3
1.0	*	*	*
1.2	*	*	*

Table C.5. Constant SNR= 6.0

Spatial Freq. (cyc./mr)	Delta -T (°C)
0.2	1.61
0.3	1.61
0.4	1.86
0.5	2.0
0.6	2.36
0.7	2.39
0.8	2.69

Table C.6. Constant Delta-T =1.94°C

Spatial Freq. (cyc./mr)	SNR
0.2	6.25
0.4	6.23
0.5	5.5
0.6	4.75
0.7	4.25
0.8	3.38

Table C.7. Constant Spatial Freq.= 0.5 cyc./mr

SNR	Delta-T (°C)
1	0.8
2	1.5
3	1.8
4	2.35
5	3.0
6	3.7
7	4.2
8	5.0

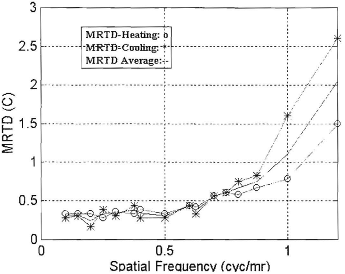

Figure C.1. Amber System Measured $MRTD_h$

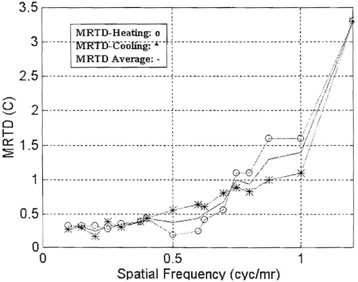

Figure C.2. Amber System Measured $MRTD_v$

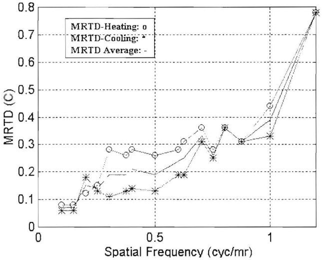

Figure C.3. Mitsubishi System Measured $MRTD_h$

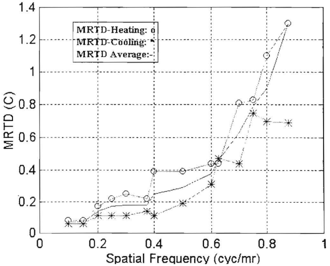

Figure C.4. Mitsubishi System Measured $MRTD_v$

APPENDIX D. FLIR92 SHORT-LISTING OUTPUTS

This Appendix shows the short-listing outputs of the FLIR92 for Amber Engineering AE4128 IR Imaging System and Mitsubishi Electronics IR-M500 Thermal Imager.

A. AMBER ENGINEERING AE4128 IR IMAGING SYSTEM

```
U.S. Army CECOM NVESD FLIR92                 Wed Sep 27 20:01:16 1995

output file:labout1.1   short listing

data file: labin1
command line arguments: -d labin1 -o labout1 -p BOTH -a labout1

begin data file listing . . .
   flir92 data file template
      >environment
         laboratory_temperature              300.0    K
         background_temperature_1            294.11   K
         BLIP_performance                    YES      YES_or_NO
      >spectral
         spectral_cut_on                     3.0      microns
         spectral_cut_off                    5.0      microns
         diffraction_wavelength              0.0      microns
      >optics_1
         eff_f_number                        3.0      --
         eff_focal_length                    10.0     cm
         eff_aperture_diameter               0.0      cm
         optics_blur_spot                    0.0      mrad
         average_optical_trans               0.0      --
      >optics_2
         HFOV:VFOV_aspect_ratio              0.0      --
         magnification                       0.0      --
         frame_rate                          109.0    Hz
         fields_per_frame                    0.0      --
```

```
>detector
  horz_dimension_(active)           40.0      microns
  vert_dimension_(active)           40.0      microns
  peak_D_star                       5.97e11   cm-sqrt(Hz)/W
  integration_time                  8887.615  microsec
  1/f_knee_frequency                0.0       Hz
>fpa_stare
  #_horz_detectors                  128.0     --
  #_vert_detectors                  128.0     --
  horz_unit_cell_dimension          50.0      microns
  vert_unit_cell_dimension          50.0      microns
>scene_phasing
  horz_target/detector_phase        0.0       degrees
  vert_target/detector_phase        0.0       degrees
>crt_display
  #_active_lines_on_CRT             480.0     --
  horz_crt_spot_sigma               0.0       mrad
  vert_crt_spot_sigma               0.0       mrad
>electronics
  high_pass_3db_cuton               0.0       Hz
  high_pass_filter_order            0.0       --
  low_pass_3db_cutoff               0.0       Hz
  low_pass_filter_order             0.0       --
  boost_amplitude                   0.0       --
  boost_frequency                   0.0       Hz
  sample_and_hold                   HORZ      HORZ_VERT_or_NO
>display
  display_brightness                10.0      milli-Lamberts
  display_height                    17.78     cm
  display_viewing_distance          88.9      cm
>eye
  threshold_SNR                     6.0       --
  eye_integration_time              0.1       sec
  MTF                               EXP       EXP_or_NL
>3d_noise_default
  noise_level                       LO        NO_LO_MOD_or_HI
>spectral_detectivity
    #_points: 3          microns____detectivity
                          3.0       0.67
                          3.34      0.8375
                          4.5       1.0
```

>end
end data file listing . . .

MESSAGES
diagnostic(): Using default 3D noise components.
diagnostic(): Using _LO_ level 3D noise defaults.
diagnostic(): Diffraction wavelength set to spectral band midpoint.
diagnostic(): Optics transmittance defaulted to 0.7.
diagnostic(): Interlace (fields per frame) defaulted to 2.
diagnostic(): Fields-of-view calculated by model.

CALCULATED SYSTEM PARAMETERS
field-of-view: 3.666h x 3.666v degrees
63.98h x 63.98v mrad
magnification: 3.116
optics blur spot: 29.280 microns (diffraction-limited)
0.293 mrad

detector IFOV: 0.400h x 0.400v mrad
FPA fill factor: 0.640
FPA duty cycle: 1.938

TEMPERATURE DEPENDENCE
BLIP detector
scaling factors (T1:300)
NETD: 1.07
peak D-star: 1.11
Planck thermal derivative: 0.83

parameter	NETD @ 300 K	NETD @ 294 K	noise bandwidth
white NETD	0.010 deg C	0.010 deg C	8.561e+001 Hz
classical NETD	0.010 deg C	0.010 deg C	8.565e+001 Hz
sigma_TVH NETD	0.008 deg C	0.008 deg C	5.629e+001 Hz
sigma_VH NETD	0.003 deg C	0.003 deg C	

Planck integral	2.127e-005	1.776e-005	W/(cm*cm*K)
. . . w/D-star	1.251e+007	1.166e+007	sqrt(Hz)/(cm*K)

TOTAL HORIZONTAL MTFs

cy/mr	H_SYS	H_PRE	H_TPF	H_SPF
0.000	1.000	1.000	1.000	1.000
0.125	0.928	0.977	1.000	0.950
0.250	0.841	0.946	1.000	0.889
0.375	0.744	0.908	1.000	0.819
0.500	0.642	0.864	1.000	0.743
0.625	0.540	0.814	1.000	0.663
0.750	0.441	0.760	1.000	0.581
0.875	0.350	0.702	1.000	0.499
1.000	0.269	0.641	1.000	0.420
1.125	0.199	0.579	1.000	0.344
1.250	0.141	0.515	1.000	0.274
1.375	0.095	0.452	1.000	0.210
1.500	0.060	0.390	1.000	0.153
1.625	0.034	0.329	1.000	0.103
1.750	0.017	0.270	1.000	0.062
1.875	0.006	0.215	1.000	0.027
2.000	0.000	0.163	1.000	0.000
2.125	0.000	0.115	1.000	-0.021
2.250	0.000	0.072	1.000	-0.035
2.375	0.000	0.034	1.000	-0.045
2.500	0.000	0.000	1.000	0.000

TOTAL VERTICAL MTFs

cy/mr	H_SYS	H_PRE	H_SPF
0.000	1.000	1.000	1.000
0.125	0.934	0.977	0.956
0.250	0.863	0.946	0.912
0.375	0.789	0.908	0.868
0.500	0.713	0.864	0.825
0.625	0.637	0.814	0.783
0.750	0.563	0.760	0.740
0.875	0.491	0.702	0.699
1.000	0.423	0.641	0.659
1.125	0.359	0.579	0.620

1.250	0.300	0.515	0.582
1.375	0.246	0.452	0.545
1.500	0.198	0.390	0.509
1.625	0.156	0.329	0.475
1.750	0.120	0.270	0.442
1.875	0.088	0.215	0.411
2.000	0.062	0.163	0.381
2.125	0.041	0.115	0.352
2.250	0.023	0.072	0.325
2.375	0.010	0.034	0.300
2.500	0.000	0.000	0.276

PREFILTER VALUES AT NYQUIST

horz H_PRE(1.00) = 0.641   vert H_PRE(1.00) = 0.641

SAMPLING RATES

horizontal	2.00 samples/mr
vertical	2.00 samples/mr
effective	2.00 samples/mr

SENSOR LIMITING FREQUENCIES

	spatial	Nyquist
horizontal	2.50	1.00
vertical	2.50	1.00
effective	2.50	1.00

MRTD 3D NOISE CORRECTION (AVERAGE)

	300 K	294 K
horizontal	1.657	1.585
vertical	1.657	1.585

MRTD AT 300 K BACKGROUND TEMPERATURE

	cy/mr	horz		cy/mr	vert	cy/mr	2D
0.05	0.125	0.001	0.05	0.125	0.001	0.127	0.001
0.10	0.250	0.003	0.10	0.250	0.003	0.150	0.002
0.15	0.375	0.005	0.15	0.375	0.004	0.174	0.002
0.20	0.500	0.007	0.20	0.500	0.006	0.197	0.002
0.25	0.625	0.010	0.25	0.625	0.008	0.221	0.002
0.30	0.750	0.013	0.30	0.750	0.011	0.244	0.003
0.35	0.875	0.019	0.35	0.875	0.014	0.277	0.003
0.40	1.000	0.027	0.40	1.000	0.018	0.314	0.004

0.45	1.125	99.999	0.45	1.125	99.999	0.351	0.004
0.50	1.250	99.999	0.50	1.250	99.999	0.391	0.005
0.55	1.375	99.999	0.55	1.375	99.999	0.439	0.005
0.60	1.500	99.999	0.60	1.500	99.999	0.486	0.006
0.65	1.625	99.999	0.65	1.625	99.999	0.538	0.007
0.70	1.750	99.999	0.70	1.750	99.999	0.591	0.008
0.75	1.875	99.999	0.75	1.875	99.999	0.646	0.009
0.80	2.000	99.999	0.80	2.000	99.999	0.702	0.011
0.85	2.125	99.999	0.85	2.125	99.999	0.762	0.012
0.90	2.250	99.999	0.90	2.250	99.999	0.823	0.014
0.95	2.375	99.999	0.95	2.375	99.999	0.882	0.016
1.00	2.500	99.999	1.00	2.500	99.999	0.936	0.019

MRTD AT 294 K BACKGROUND TEMPERATURE

	cy/mr	horz		cy/mr	vert	cy/mr	2D
0.05	0.125	0.001	0.05	0.125	0.001	0.127	0.001
0.10	0.250	0.003	0.10	0.250	0.003	0.150	0.002
0.15	0.375	0.005	0.15	0.375	0.005	0.174	0.002
0.20	0.500	0.007	0.20	0.500	0.006	0.197	0.002
0.25	0.625	0.010	0.25	0.625	0.009	0.221	0.002
0.30	0.750	0.014	0.30	0.750	0.011	0.244	0.003
0.35	0.875	0.019	0.35	0.875	0.015	0.277	0.003
0.40	1.000	0.028	0.40	1.000	0.019	0.314	0.004
0.45	1.125	99.999	0.45	1.125	99.999	0.351	0.004
0.50	1.250	99.999	0.50	1.250	99.999	0.391	0.005
0.55	1.375	99.999	0.55	1.375	99.999	0.439	0.006
0.60	1.500	99.999	0.60	1.500	99.999	0.486	0.006
0.65	1.625	99.999	0.65	1.625	99.999	0.538	0.007
0.70	1.750	99.999	0.70	1.750	99.999	0.591	0.008
0.75	1.875	99.999	0.75	1.875	99.999	0.646	0.010
0.80	2.000	99.999	0.80	2.000	99.999	0.702	0.011
0.85	2.125	99.999	0.85	2.125	99.999	0.762	0.013
0.90	2.250	99.999	0.90	2.250	99.999	0.823	0.015
0.95	2.375	99.999	0.95	2.375	99.999	0.882	0.017
1.00	2.500	99.999	1.00	2.500	99.999	0.936	0.019

MDTD AT 300 K BACKGROUND TEMPERATURE

	1/mr	MDTD
0.20	12.500	1.232
0.40	6.250	0.315
0.60	4.167	0.145
0.80	3.125	0.086

1.00	2.500	0.058
1.20	2.083	0.043
1.40	1.786	0.034
1.60	1.563	0.028
1.80	1.389	0.023
2.00	1.250	0.020
2.20	1.136	0.018
2.40	1.042	0.016
2.60	0.962	0.014
2.80	0.893	0.013
3.00	0.833	0.012
3.20	0.781	0.011
3.40	0.735	0.010
3.60	0.694	0.010
3.80	0.658	0.009
4.00	0.625	0.009
4.20	0.595	0.008
4.40	0.568	0.008
4.60	0.543	0.007
4.80	0.521	0.007
5.00	0.500	0.007

MDTD AT 294 K BACKGROUND TEMPERATURE

	1/mr	MDTD
0.20	12.500	1.266
0.40	6.250	0.324
0.60	4.167	0.149
0.80	3.125	0.088
1.00	2.500	0.060
1.20	2.083	0.044
1.40	1.786	0.035
1.60	1.563	0.028
1.80	1.389	0.024
2.00	1.250	0.021
2.20	1.136	0.018
2.40	1.042	0.016
2.60	0.962	0.015
2.80	0.893	0.013
3.00	0.833	0.012
3.20	0.781	0.011
3.40	0.735	0.011

3.60	0.694	0.010
3.80	0.658	0.009
4.00	0.625	0.009
4.20	0.595	0.008
4.40	0.568	0.008
4.60	0.543	0.008
4.80	0.521	0.007
5.00	0.500	0.007

FLIR92. . . labout1.1: end of listing

B. MITSUBISHI ELECTRONICS IR-M500 THERMAL IMAGER

U.S. Army CECOM NVESD FLIR92 Thu Sep 28 09:11:44 1995

output file: mitsh.1 short listing

data file: mitsh
command line arguments: -d mitsh -o mitsh -p BOTH -a mitsh

begin data file listing . . .
flir92 data file template

>environment		
laboratory_temperature	300.0	K
background_temperature_1	294.0	K
BLIP_performance	YES	YES_or_NO
>spectral		
spectral_cut_on	3.0	microns
spectral_cut_off	5.0	microns
diffraction_wavelength	0.0	microns
>optics_1		
eff_f_number	1.4	--
eff_focal_length	5.0	cm
eff_aperture_diameter	0.0	cm
optics_blur_spot	0.0	mrad
average_optical_trans	0.95	--
>optics_2		
HFOV:VFOV_aspect_ratio	0.0	--
magnification	0.0	--

frame_rate	60.0	Hz
fields_per_frame	1.0	--
>detector		
horz_dimension_(active)	16.24	microns
vert_dimension_(active)	12.49	microns
peak_D_star	5.0e10	cm-sqrt(Hz)/W
integration_time	16145.833	microsec
1/f_knee_frequency	0.0	Hz
>fpa_stare		
#_horz_detectors	512	--
#_vert_detectors	512	--
horz_unit_cell_dimension	26	microns
vert_unit_cell_dimension	20	microns
>PtSi		
emission_coefficient	0.16	1/eV
Schottky_barrier_height	0.22	eV
>electronics		
high_pass_3db_cuton	0.0	Hz
high_pass_filter_order	0.0	--
low_pass_3db_cutoff	0.0	Hz
low_pass_filter_order	0.0	--
boost_amplitude	0.0	--
boost_frequency	0.0	Hz
sample_and_hold	HORZ	HORZ_VERT_or_NO
>display		
display_brightness	10.0	milli-Lamberts
display_height	27.94	cm
display_viewing_distance	88.9	cm
>crt_display		
#_active_lines_on_CRT	480	--
horz_crt_spot_sigma	0.0	mrad
vert_crt_spot_sigma	0.0	mrad
>eye		
threshold_SNR	6.0	--
eye_integration_time	0.2	sec
MTF	EXP	EXP_or_NL
>3d_noise_default		
noise_level	MOD	NO_LO_MOD_or_HI
>end		

end data file listing . . .

MESSAGES

diagnostic(): Using default 3D noise components.
diagnostic(): Using _LO_ level 3D noise defaults.
diagnostic(): Diffraction wavelength set to spectral band midpoint.
diagnostic(): Fields-of-view calculated by model.
diagnostic(): PtSi spectral detectivity predicted by model.

CALCULATED SYSTEM PARAMETERS

field-of-view:	15.166h x 11.694v degrees
	264.68h x 204.09v mrad
magnification:	1.527
optics blur spot:	13.664 microns (diffraction-limited)
	0.273 mrad
detector IFOV:	0.325h x 0.250v mrad
FPA fill factor:	0.390
FPA duty cycle:	0.969

NORMALIZED DETECTOR SPECTRAL DETECTIVITY

wavelength	detectivity
3.00	1.00
3.22	0.78
3.44	0.60
3.67	0.46
3.89	0.34
4.11	0.24
4.33	0.17
4.56	0.11
4.78	0.07
5.00	0.03

TEMPERATURE DEPENDENCE

BLIP detector
scaling factors (T1:300)
NETD: 1.10
peak D-star: 1.12
Planck thermal derivative: 0.83

parameter	NETD @ 300 K	NETD @ 294 K	noise bandwidth
---------	------------ ------------	---------------	
white NETD	0.200 deg C	0.221 deg C	4.712e+001 Hz
classical NETD	0.200 deg C	0.221 deg C	4.714e+001 Hz
sigma_TVH NETD	0.162 deg C	0.179 deg C	3.101e+001 Hz
sigma_VH NETD	0.065 deg C	0.065 deg C	
Planck integral	2.127e-005	1.769e-005	W/(cm*cm*K)
. . . w/D-star	1.986e+005	1.802e+005	sqrt(Hz)/(cm*K)

TOTAL HORIZONTAL MTFs

cy/mr	H_SYS	H_PRE	H_TPF	H_SPF
0.000	1.000	1.000	1.000	1.000
0.154	0.850	0.974	1.000	0.872
0.308	0.679	0.940	1.000	0.721
0.462	0.509	0.900	1.000	0.566
0.616	0.358	0.853	1.000	0.419
0.770	0.235	0.802	1.000	0.294
0.924	0.144	0.746	1.000	0.193
1.078	0.081	0.686	1.000	0.119
1.232	0.042	0.624	1.000	0.068
1.385	0.020	0.561	1.000	0.035
1.539	0.008	0.498	1.000	0.016
1.693	0.003	0.434	1.000	0.006
1.847	0.000	0.373	1.000	0.001
2.001	0.000	0.313	1.000	-0.001
2.155	0.000	0.256	1.000	-0.001
2.309	0.000	0.202	1.000	-0.001
2.463	0.000	0.153	1.000	-0.001
2.617	0.000	0.107	1.000	-0.000
2.771	0.000	0.067	1.000	-0.000
2.925	0.000	0.031	1.000	-0.000
3.079	0.000	0.000	1.000	0.000

TOTAL VERTICAL MTFs

cy/mr	H_SYS	H_PRE	H_SPF
0.000	1.000	1.000	1.000
0.200	0.816	0.967	0.843

0.400	0.626	0.927	0.674
0.600	0.450	0.881	0.511
0.801	0.304	0.829	0.367
1.001	0.193	0.772	0.250
1.201	0.115	0.712	0.162
1.401	0.064	0.649	0.099
1.601	0.034	0.585	0.057
1.801	0.016	0.520	0.032
2.002	0.008	0.456	0.016
2.202	0.003	0.394	0.008
2.402	0.001	0.334	0.004
2.602	0.000	0.277	0.002
2.802	0.000	0.223	0.001
3.002	0.000	0.174	0.000
3.203	0.000	0.129	0.000
3.403	0.000	0.090	0.000
3.603	0.000	0.055	0.000
3.803	0.000	0.025	0.000
4.003	0.000	0.000	0.000

PREFILTER VALUES AT NYQUIST

horz H_PRE(0.96) = 0.731 vert H_PRE(1.25) = 0.696

SAMPLING RATES

horizontal	1.92 samples/mr
vertical	2.50 samples/mr
effective	2.19 samples/mr

SENSOR LIMITING FREQUENCIES

	spatial	Nyquist
horizontal	3.08	0.96
vertical	4.00	1.25
effective	3.51	1.10

MRTD 3D NOISE CORRECTION (AVERAGE)

	300 K	294 K
horizontal	1.709	1.606
vertical	1.709	1.606

MRTD AT 300 K BACKGROUND TEMPERATURE

	cy/mr	horz		cy/mr	vert	cy/mr	2D
0.05	0.154	0.032	0.05	0.200	0.042	0.203	0.042
0.10	0.308	0.073	0.10	0.400	0.098	0.239	0.050
0.15	0.462	0.132	0.15	0.600	0.183	0.275	0.060
0.20	0.616	0.227	0.20	0.801	0.325	0.311	0.071
0.25	0.770	0.394	0.25	1.001	0.582	0.352	0.084
0.30	0.924	0.713	0.30	1.201	1.064	0.395	0.099
0.35	1.078	99.999	0.35	1.401	99.999	0.444	0.117
0.40	1.232	99.999	0.40	1.601	99.999	0.494	0.139
0.45	1.385	99.999	0.45	1.801	99.999	0.545	0.165
0.50	1.539	99.999	0.50	2.002	99.999	0.597	0.195
0.55	1.693	99.999	0.55	2.202	99.999	0.651	0.231
0.60	1.847	99.999	0.60	2.402	99.999	0.703	0.274
0.65	2.001	99.999	0.65	2.602	99.999	0.756	0.325
0.70	2.155	99.999	0.70	2.802	99.999	0.809	0.385
0.75	2.309	99.999	0.75	3.002	99.999	0.860	0.456
0.80	2.463	99.999	0.80	3.203	99.999	0.911	0.540
0.85	2.617	99.999	0.85	3.403	99.999	0.961	0.640
0.90	2.771	99.999	0.90	3.603	99.999	1.004	0.758
0.95	2.925	99.999	0.95	3.803	99.999	1.032	0.898
1.00	3.079	99.999	1.00	4.003	99.999	1.060	1.064

MRTD AT 294 K BACKGROUND TEMPERATURE

	cy/mr	horz		cy/mr	vert	cy/mr	2D
0.05	0.154	0.033	0.05	0.200	0.044	0.203	0.044
0.10	0.308	0.075	0.10	0.400	0.102	0.239	0.052
0.15	0.462	0.137	0.15	0.600	0.190	0.275	0.062
0.20	0.616	0.236	0.20	0.801	0.337	0.311	0.073
0.25	0.770	0.409	0.25	1.001	0.603	0.352	0.087
0.30	0.924	0.739	0.30	1.201	1.103	0.395	0.103
0.35	1.078	99.999	0.35	1.401	99.999	0.444	0.122
0.40	1.232	99.999	0.40	1.601	99.999	0.494	0.144
0.45	1.385	99.999	0.45	1.801	99.999	0.545	0.171
0.50	1.539	99.999	0.50	2.002	99.999	0.597	0.202
0.55	1.693	99.999	0.55	2.202	99.999	0.651	0.240
0.60	1.847	99.999	0.60	2.402	99.999	0.703	0.284
0.65	2.001	99.999	0.65	2.602	99.999	0.756	0.336
0.70	2.155	99.999	0.70	2.802	99.999	0.809	0.399
0.75	2.309	99.999	0.75	3.002	99.999	0.860	0.472

0.80	2.463	99.999	0.80	3.203	99.999	0.911	0.559
0.85	2.617	99.999	0.85	3.403	99.999	0.961	0.663
0.90	2.771	99.999	0.90	3.603	99.999	1.004	0.785
0.95	2.925	99.999	0.95	3.803	99.999	1.032	0.931
1.00	3.079	99.999	1.00	4.003	99.999	1.060	1.103

MDTD AT 300 K BACKGROUND TEMPERATURE

	1/mr	MDTD
0.20	17.554	60.173
0.40	8.777	15.142
0.60	5.851	6.803
0.80	4.388	3.884
1.00	3.511	2.532
1.20	2.926	1.797
1.40	2.508	1.354
1.60	2.194	1.066
1.80	1.950	0.868
2.00	1.755	0.726
2.20	1.596	0.620
2.40	1.463	0.539
2.60	1.350	0.476
2.80	1.254	0.425
3.00	1.170	0.384
3.20	1.097	0.350
3.40	1.033	0.321
3.60	0.975	0.297
3.80	0.924	0.276
4.00	0.878	0.258
4.20	0.836	0.242
4.40	0.798	0.228
4.60	0.763	0.215
4.80	0.731	0.204
5.00	0.702	0.194

MDTD AT 294 K BACKGROUND TEMPERATURE

	1/mr	MDTD
0.20	17.554	62.351
0.40	8.777	15.690
0.60	5.851	7.049
0.80	4.388	4.024
1.00	3.511	2.624
1.20	2.926	1.863
1.40	2.508	1.403
1.60	2.194	1.104
1.80	1.950	0.899
2.00	1.755	0.752
2.20	1.596	0.643
2.40	1.463	0.559
2.60	1.350	0.493
2.80	1.254	0.441
3.00	1.170	0.398
3.20	1.097	0.363
3.40	1.033	0.333
3.60	0.975	0.308
3.80	0.924	0.286
4.00	0.878	0.267
4.20	0.836	0.251
4.40	0.798	0.236
4.60	0.763	0.223
4.80	0.731	0.211
5.00	0.702	0.201

FLIR92. . . mitsh.1: end of listing

LIST OF REFERENCES

1. J. M. Lloyd, Thermal Imaging Systems, Chapter 1, 5, Plenum Press, New York, 1975.

2. Gerald C. Holst, Electro-optical Imaging System Performance, Chapter 4, 19, 20, SPIE Optical Engineering Press, Bellingham, 1995.

3. Alejandro R. Ugarte, "Modeling for Improved Minimum Resolvable Temperature Difference Measurements", Master's Thesis in Electrical Engineering, Naval Postgraduate School, September, 1991.

4. J. A. Ratches, "Static Performance Model for Thermal Imaging Systems", Optical Engineering, Vol. 15, No. 6, pp. 525-530, 1976.

5. J. G. Vortman, A. Ber-Lev, "Improved Minimum Resolvable Temperature Difference Model for Infrared Imaging Systems", Optical Engineering, Vol. 26, No. 6, pp. 492-498, 1987.

6. W. R. Lawson, J. A. Ratches, "The Night Vision Laboratory Static Performance Model Based on the Matched Filter Concept", NRL REPORT 8311, Appendix C, pp. 159-179, Electro-Optical Technology Program Office,Washington D. C., 1979.

7. M. L. Gao, M. A. Karim, S. H. Zheng, "Device Nonspecific Minimum Resolvable Temperature Difference for Infrared Imaging Systems Characterization", Optical Engineering, Vol.29, No.8, pp.905-910, 1990.

8. Ron J. Pieper, Alfred W. Cooper, "A Visibility Model for MRTD Prediction", Proceedings SPIE, Vol. 224, Infrared Imaging Systems: Design, Analysis, Modeling, and Testing V, pp. 259-269, April 1994.

9. U.S. Army Night Vision and Electronic Sensors Directorate, "FLIR92 Thermal Imaging Systems Performance Model", Analyst's Reference Guide, January 1993.

10. U.S. Army Night Vision and Electronic Sensors Directorate, "FLIR92 Thermal Imaging Systems Performance Model", User's Guide, January 1993.

11. John A. D' Agostino, " A 3-D Noise Analysis Methodology", FLIR92 Thermal Imaging Systems Performance Model Analyst's Reference Guide, Appendix A, pp. ARG_15-22, March 1991.

12. Curtis M. Webb, Paul A. Bell, "Laboratorty Procedure for the Characterization of 3-D Noise in Thermal Imaging Systems", FLIR92 Thermal Imaging Systems Performance Model Analyst's Reference Guide, Appendix B, pp. ARG_23-30, March 1991.

13. Luke Scott, John A. D.' Agostino, "Application of 3-D Noise to MRTD Prediction", FLIR92 Thermal Imaging Systems Performance Model Analyst's Reference Guide, Appendix C, pp. ARG_31-38, February 1992.

14. Curtis M. Webb, "An Approach to 3-Dimensional Noise Spectral Analysis", SPIE, Vol. 2470, pp. 288-299, 1995.

15. Jonathan M. Mooney, "Effects of Spatial Noise on the Minimum Resolvable Temperature of a Staring Sensor", Applied Optics, Vol. 30, No. 23, August 1991.

16. Duke Scott, John D.' Agostino, "NVEOD FLIR92 Thermal Imaging Systems Performance Model", SPIE, Vol. 1689 Infrared Imaging Systems, pp. 194-203, 1992.

17. F. O. Huck, N. Halyo, S. K. Park, " Aliasing and Blurring in 2-D Sampled Imagery", Applied Optics, Vol.19, No: 13, p. 2174-2181, 1 July 1991.

18. Edward A. Watson, Robert A. Muse, Fred P. Blommel, " Aliasing and Blurring in Microscanned Imagery", SPIE, Vol. 1689, Infrared Imaging Systems, p. 242-250, September 1992.

19. Mark A. Chambliss, James A. Dawson, Eric J. Borg, " Measuring the MTF of Undersampled Staring IRFPA Sensors Using 2D Discrete Fourier Transform", SPIE Vol. 2470, p. 312-324, April 1995.

20. E. G. D. Youngs, R. K. McEwen, "A Performance Prediction and Simulation Model for 2 Dimensional Array Imagers", Fourth International Conference on Advanced Infrared Detectors and Systems Conf. Publication, No. 321, p. 171-182, IEE London 1990.

21. T. L. Williams, N. T. Davidson, S. Wocial, " Results of Some Preliminary work on Objective MRTD Measurement", SPIE, Vol. 549 Image Quality: An Overview, p. 44-49, 1985.

22. T. L. Williams, "Image Assessment Infrared and Visible", SPIE, Vol. 467 Image Assessment: Infrared and Visible, p. 47-54, 1983.

23. A. R. Newbery, R. M. Mc Mahon, "Use of Minimum Resolvable Temperature Difference (MRTD) for the Evaluation and Specification of Thermal Imaging Systems", SPIE, Vol. 274 Assessment of Imaging Systems: Visible and Infrared, p. 268-272, 1981.

24. Amber Engineering, Inc. , AE4128 Infrared Imaging System Manual, March 1992.

25. Amber Engineering, Inc. , AE4128 Software System Manual, Mach 1992.

26. Mitsibushi Electronics America, Inc., IR-M500 Thermal Imager User's Guide, 1992.

27. M. Groen, "Development and Validation of a Second Generation Visibility-Based Model for Predicting Subjective and Objective Minimum Resolvable Temperature Difference Performance for Staring Thermal Imaging Systems", Master's Thesis in Electrical Engineering, Naval Postgraduate School, December 1995.

28. J. M. Mooney, "Effects of Spatial Noise on the Minimum Resolvable Temperature of a Staring Sensor", Applied Optics, Vol.30, No. 23, 10 August 1991.

29. J. A. Ratches, J. D. Howe, "FLIR Modeling Workshop Report", Procs. IRIS Passive Sensors, Vol.1, p. 223-234, 1990.

30. T. Meitzler, G. Gerhart, "Spatial Aliasing in Ground Vehicle IR Imagery", SPIE, Vol. 1689 Infrared Imaging Systems, p. 226-240, 1992.

31. S. K. Park, R. Schowengerdt, M. Kaczynski, "Modulation-transfer-function Analysis for Sampled Image Systems", Applied Optics, Vol. 23, No. 15, p. 2572-2582, 1 August 1984.

32. Leo O. Vroombout, "Second Generation Thermal Imaging System Design Trades Modeling", SPIE, Vol. 1309 Infrared Imaging Systems: Design, Analysis, Modeling, and Testing, 1990.

33. A. D. Schnitzler, "Image-detector Model and Parameters of the Human Visual System", Journal of the Optical Society of America, Vol. 63, p. 1357-1368.

34. G. H. Kornfeld, W. R. Lawson,"Visual-Perception Models", J. Optical Soc. Am. , Vol. 61, No. 6, p. 811-820, 1971.

35. A. D. Schnitzler, "Theory of Spatial-frequency Filtering by the Human Visul System. II. Performance Limited by Video Noise", J. Optical Soc. Am., Vol. 66, No. 6, p. 617-625, 1976.

36. F. W. Cambell,"The Human Eye as an Optical Filter", Proceedings of the IEEE , Vol. 56, No. 6, p. 1009-1014, 1968.

37. Ferrel G. Stremler, Introduction to Communication Systems, Third Edition, Adisor Wesley, 1990.

38. J. W. Goodman, Introduction to Fourier Optics, McGraw-Hill, New York, 1968.

INITIAL DISTRIBUTION LIST

		No. of Copies
1.	Defense Technical Information Center 8725 John J. Kingman Rd., STE 0944 Ft. Belvoir, Virginia 22060-6218	2
2.	Library Code 013 Naval Postgraduate School Monterey, California 93943-5002	2
3.	Chairman, Electronic Warfare Academic Group, Code EW Naval Postgraduate School Monterey, California 93943	1
4.	Professor Ron J. Pieper, Code EC/PR Department of Electrical and Computer Engineering Naval Postgraduate School Monterey, California 93943	3
5.	Professor Alfred W. Cooper Code PH/CR Department of Physics Naval Postgraduate School Monterey, California 93943	1
6.	Turk Deniz Kuvvetleri Komutanligi Bakanliklar - Ankara Turkey	2
7.	LTJG. Cem Koc Sair Necati Sok. No: 15/1 80840 Ortakoy - Istanbul Turkey	2